POLYANILINE BASED COMPOSITE MEMBRANES FOR PEM FUEL CELLS:

EXPERIMENTS AND FACTORIAL DESIGN

by

Ahmed Eisa

A Thesis presented to the Faculty of the
American University of Sharjah
College of Engineering
In Partial Fulfillment
of the Requirements
for the Degree of

Master of Science in
Chemical Engineering

Sharjah, United Arab Emirates

December 2020

Declaration of Authorship

I declare that this thesis is my own work and, to the best of my knowledge and belief, it does not contain material published or written by a third party, except where permission has been obtained and/or appropriately cited through full and accurate referencing.

Signed……Ahmed Eisa…….

Date……11/10/20……..

Approval Signatures

We, the undersigned, approve the Master's Thesis of Ahmed Eisa

Thesis Title: Polyaniline Based Composite Membranes for PEM Fuel Cells: Experiments and Factorial Design.

Date of Defense: 22/11/2020.

Name, Title and Affiliation	Signature
Dr. Amani Al-Othman Associate Professor, Department of Chemical Engineering Thesis Advisor	
Dr. Mohammad Al-Sayah Professor, Department of Biology, Chemistry and Environmental Sciences Thesis Co-Advisor	
Dr. Yassir Makkawi Professor, Department of Chemical Engineering Thesis Committee Member	
Dr. Sameer Al-Asheh Professor, Department of Chemical Engineering Thesis Committee Member	
Dr. Sameer Al-Asheh Head Department of Chemical Engineering	
Dr. Lotfi Romdhane Associate Dean for Graduate Studies and Research College of Engineering	
Dr. Sirin Tekinay Dean College of Engineering	
Dr. Mohamed El-Tarhuni Vice Provost for Graduate Studies Office of Graduate Studies	

Acknowledgement

I would like to show my greatest appreciation for my advisors; Dr. Amani Al-Othman and Dr. Mohammad Al-Sayah for standing by my side ever since the beginning of this work. They provided me with academic, technical and psychological support throughout that period. They were very appealing and they made everything look easier no matter how hard it was.

In addition, I would also want to thank our lab instructors; Eng. Muhammad Qasim, Eng. Najla Salkho and Eng. Mohammed Badrelzaman for providing technical support in the working area and teaching me about the different equipment and how to use them. They also made sure my samples are well-stored and away from other students' hands in my absence.

Furthermore, I would like to thank my professors; Dr. Naif Darwish and Dr. Ghaleb Husseini for their encouragement to join the Master's program. In addition, I would like to acknowledge everyone who was involved in the decision of me being awarded the graduate teaching assistantship merit.

Special gratitude also for Dr. Sameer Al-Asheh (Head of the Chemical Engineering Department) for his continues support. His advices were priceless and his efforts were countless. He never gave up on me and his guidance was very crucial and important to me.

My appreciation is also extended to Dr. Lotfi Ramdhane (Associate Dean for Graduate Affairs and Research) for being very understanding. His communications and guidance when it comes to graduate affairs were beyond phenomenal.

Last but not least, I would like to thank everyone in my collage; starting from faculty members, all the way to my colleagues. Every single one of them has made my life much easier in this university. I cannot be thankful enough for your support. You are the ones who made all of this possible. Gracias.

Abstract

Higher temperature operation (higher than 100 ^{o}C) in proton exchange membrane fuel cells (PEMFCs) is preferred and has several advantages including enhanced fuel cell kinetics, improved catalysts tolerance for contaminants and recovery of useful heat. However, high temperature operation is not permitted using the conventional Nafion membranes as they dehydrate and their proton conductivity dramatically decreases. In this thesis, novel proton conductors based on polyaniline (PANI), ionic liquids (ILs) and zirconium phosphate (ZrP) were fabricated and proposed for the higher temperature operation in PEMFCs. PANI-IL-ZrP composite membranes were synthesized using polytetrafluoroethylene (PTFE) as support. These composite membranes were evaluated for their proton conductivity. The membrane synthesis results showed a promising proton conductivity of around 0.02 S/cm for PANI/IL/ZrP composite membrane as well as high thermal stability at 180 ^{o}C. The membranes' performance was assessed by generating theoretical polarization curves. The results demonstrated a promising cell performance with a current density of 0.042 A/cm^2 at a cell potential of 0.6 V that are comparable to the methanol fuel cell. The membrane parameters that affect the performance of fuel cells at high temperature operation were also studied and optimized using factorial design (FD) modeling approach. The studied parameters were the concentrations of PANI, IL and ZrP in addition to the operating temperature and the IL type. The modelling results showed that the concentration of 1-Hexyl-3-Methylimidazolium Tricyanomethanide (HMT) IL contributes approximately to 50% of the conductivity response. The optimization of parameters performed in this thesis offer an important basis as a rational of high temperature PEMFC design.

Keywords: ***High temperature fuel cells; factorial design; polyaniline; proton exchange membrane fuel cell (PEMFC); ionic liquids (IL); composite membranes.***

Table of Contents

List of Figures

List of Tables

List of Abbreviations

AFC	Alkaline Fuel Cell
Coef	Coefficient
CTA	Cellulose Triacetate
DC	Direct Current
DEMM	Diethylmethylammonium Methanesulfonate
DMFC	Direct Methanol Fuel Cell
DTA	N-Dodecyltriethylammonium
EB	Emeraldine Base
EIS	Electrochemical Impedance Spectroscopy
ES	Emeraldine Salt
FC	Fuel Cell
FD	Factorial Design
GCC	Gulf Cooperation Council
GmbH	Gesellschaft mit beschränkter Haftung
HEMA	Hydroxyethylmethacrylate
HMT	1-Hexyl-3-Methylimidazolium Tricyanomethanide
IL	Ionic Liquid

IoLitTec	Ionic Liquid Technology
KPS	Potassium Persulfate
MCFC	Molten Carbonate Fuel Cell
MMA	Methyl Methacrylate
M-PANI	Meta-Polyaniline
PANI	Polyaniline
PBI	polybenzimidazole
PEM	Polymer Electrolyte Membrane
PEMFC	Proton Exchange Membrane Fuel Cell
PTFE	Polytetrafluoroethylene
PVdF	Polyvinylidene Difluoride
SDS	Sodium Dodecyl Sulphate
SE	Standard Error
SOFC	Solid Oxide Fuel Cell
SPAEK-C	Sulfonated Poly-Arylene-Ether-Ketone Bearing Carboxyl Groups
SPEEK	Sulfonated Polyether-Ether Ketone
SS	Sum of the Squares
ZrP	Zirchomium Phosphate

Chapter 1. Introduction

This chapter provides a general overview of fuel cells; their types and applications. It also addresses the main drawbacks of low temperature operations in fuel cells and the need to develop new membranes that can withstand high temperature operations. The research contributions followed by the organization of the remaining chapters of the thesis are also provided in this chapter.

1.1. Overview

Sustainable energy generation represents a significant challenge since it is linked hand in hand with human and environment protection. Ozone depletion, hazardous pollutants emissions, climate change and global warming are all critical problems arise from conventional (fossil fuel based) energy generation [1]. As a result of the massive increase in energy demand, the world is approaching a serious global power crisis [2]. According to the International Energy Agency (IEA) report in 2014, residents' consumption of electricity is increasing rapidly in GCC countries as can be seen from Figure 1 [3].

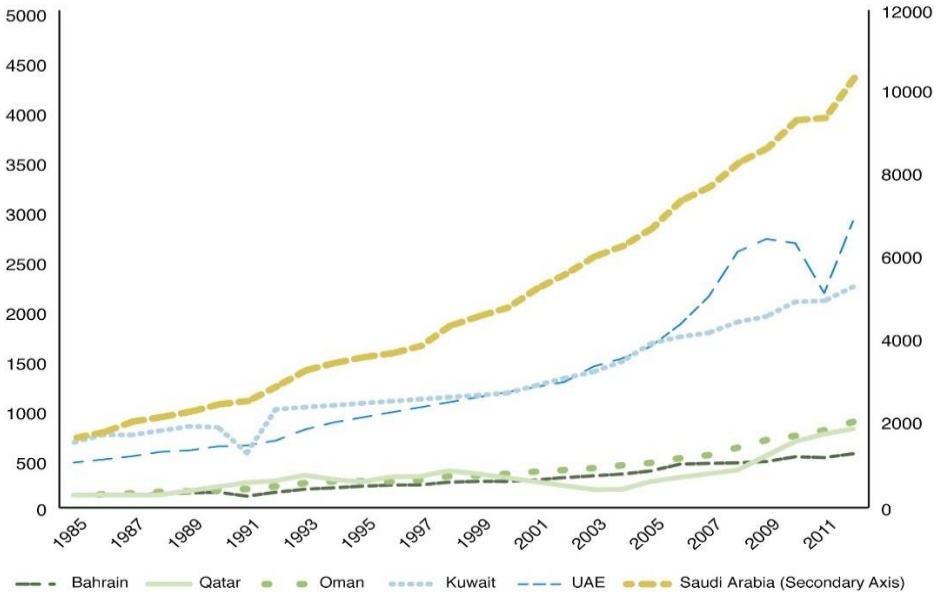

Figure 1: Electricity consumption in killotonne of oil equivalent (left y-axis) for the GCC countries from 1985 to 2012 (x-axis). (Saudi Arabia is on the right y-axis) [3].

In order to meet the high consumers demand, an alternative environmentally-friendly energy source must be implemented. Fuel cells (FCs) are considered to be one of the promising systems for power generation. They have been investigated intensively in the past decade. Fuel cells are finding their way in variety of applications such as: automobiles, buildings cogeneration and standby power supply [4]. They are preferred due to their high efficiency, excellent power density, all solid structure and their zero greenhouse gasses emissions (if the fuel is hydrogen) [5]. In addition, fuel cell systems are compatible with renewable energy carries (i.e. hydrogen), easy to assemble and operate, have diversity of applications and do not generate noises [6]. Unlike internal combustion systems, fuel cells provide clean and efficient approach for the conversion of energy [6].

In a fuel cell system, chemical energy is converted into an electric power via the electro-oxidation of the fuel. The system consists of two electrodes (usually made of platinum on carbon), separated via a dense membrane that only allow the passage of protons. The two electrodes are connected electrically through an external wire/load for the flow of electrons. The flow of electrons results in an electric current. The fuel cell is similar to the battery in producing DC current, but different in a way that fuel is continuously injected to the anode (negative electrode), while oxygen is fed to the cathode (positive electrode) on the other side as electron acceptor.

There are many types of fuel cells depending on the types of fuel and membranes being used in the cell. They are usually classified based on their electrolyte material. Some of the available FCs in the market include: proton exchange membrane fuel cell (PEMFC), direct methanol Fuel Cell (DMFC), alkaline fuel cell (AFC), solid oxide fuel cell (SOFC), and molten carbonate fuel cell (MCFC) and many more [6]. Among all, the most promising cell is the PEMFC [7].

The working principle of PEMFC is described in Figure 1, where hydrogen is used as a fuel, however natural gas and some hydrocarbons may also be used [8]. Initially, hydrogen is introduced to the anode side where it gets oxidized on the catalyst (platinum) to produce electrons and protons. After electro-oxidation, electrons move through an

external wire/circuit from the anode to the cathode; whereas protons travel through the membrane via the hoping (Grotthus) mechanism [9].

In principle, protons adhere to the available water molecules in the membrane forming hydronium ions (H_3O^+) and diffuse through the membrane toward the cathode. At the cathode, oxygen is introduced, accepts the electrons and reduces on the catalyst (platinum) to form O^{-2}. The O^{-2} then combines with the migrating protons in the membrane to form water and complete the circuit.

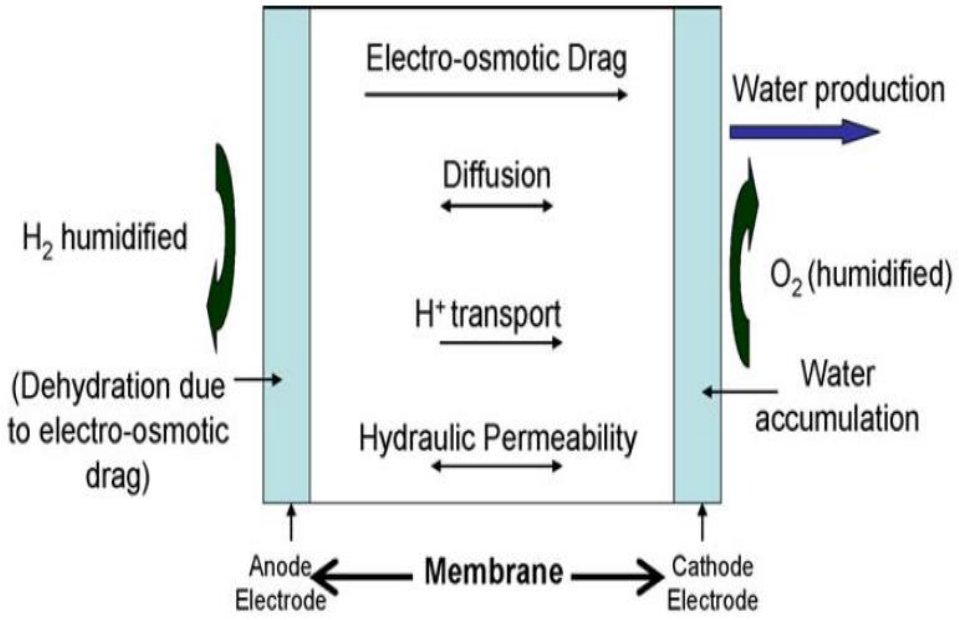

Figure 2: H_2/O_2 fuel cell [12].

The most widely used membranes in PEMFCs are perfluorosulfonic acid polymer membranes, e.g Nafion of DuPont [10]. It has a conductivity of 0.1 S/cm at room temperature [10]. However, the main drawback of Nafion based membranes is that they can operate efficiently only at a low temperature (around 80 ^oC) [11] and their conductivity strongly depends on water content. Beyond this temperature, the membrane dehydrates resulting in a remarkable decrease in proton conductivity. Therefore, high temperature operation is preferred on PEM fuel cells.

Many features are associated with the implementation of high temperature PEMFCs including: improved cathode kinetics, enhanced tolerance of the catalyst to contaminants, improved water management and gas transport [12]. Therefore, there is a need to develop Nafion- alternative membrane materials. Polymer electrolyte membranes (PEMs) should be thermally and mechanically stable, have the ability to retain water and should allow proton-crossover by having available proton-exchange sites or water molecules [13].

Several polymers and materials were investigated as Nafion alternatives in the literature such as polybenzimidazole (PBI) family, polyaniline (PANI), sulfonated polyether-ether ketone (SPEEK) and cellulose based membranes [14]. These membranes are believed to accommodate more than one of the previously addressed PEMs' criteria. PANI has been used in Nafion membranes and showed promising results [15]. Zirconium phosphate was also highly investigated in literature and presented remarkable conductivity results [16]. Ionic liquids have been also incorporated into Nafion and other polymer membranes and showed improved conductivity [17].

1.2. Thesis Objectives

The objective of this work is to develop a composite proton exchange membrane that can sustain high temperature operation in PEMFC applications. Therefore, several composite membranes based on polyaniline (PANI), zirchonuim phosphate (ZrP) and ionic liquid (IL) were synthesized. The membranes were fabricated over polytetrafluoroethylene (PTFE) sheets. The fabricated membranes will be tested and characterized in a sample stainless steel cell rather than incorporating them in an actual fuel cell.

In addition, this work aims to develop a factorial design (FD) model that would help assessing the factors that affect the conductivity of the synthesized membranes. The FD model will study how the concentration of the used materials in addition to the type of IL used and the operating temperature would affect the conductivity response of the membranes.

Another purpose of this thesis is to study the performance of the characterized fuel cell. This would be accomplished by generating theoretical polarization curves. The curves

will show the cell potential/current density relationship, which will give an understanding about the stability/degradation of the synthesized membranes. The optimum goal is to reach a thermally-stable conductive membrane based on the previously mentioned materials.

1.3. Research Contribution

The contributions of this thesis is due to the following:

- Propose a novel Nafion-free membrane that can withstand high temperature operations in order to avoid membrane dehydration problems, achieve faster kinetics and avoid catalyst poisoning.
- Propose a tool on factorial design modelling to identify the key factors affecting membrane conductivity and the contribution of each factor to the conductivity response.
- Propose an approach to predict fuel cell performance via generating theoretical polarization curves.

1.4. Thesis Organization

The following sections of this thesis work is organized as follows: Chapter 2 will discuss some background information and research work about PANI, ZrP and IL based membranes. It will focus on their chemistry and their ability to conduct protons. After that, Chapter 3 will discuss the experimental and theoretical approaches used in this work along with the modelling equations. Next, Chapter 4 will provide the conductivity, factorial design and cell performance results. It will also discuss the main findings compared to literature. Finally, Chapter 5 will concludes this work and provides a potential for future work.

Chapter 2. Background and Literature Review

This section presents the significance of fuel cells' membranes operating at elevated temperatures. First of all, it discusses the chemistry and the properties of each material involved in the new suggested membrane (polyaniline/zirconium phosphate/ionic liquid (PANI/ZrP/IL) supported by polytetrafluoroethylene (PTFE).

The chapter also investigates the performance of each material individually as part of a fuel cell systems. In addition, it provides an up to date literature on the proton conductivity and the performance of composite membranes based on the materials mentioned earlier.

Furthermore, the chapter looks at factorial design (FD) modelling and how it can be incorporated when it comes to fuel cells. It shows how FD can be used to determine the key factors that affect the fuel cell performance. It also shows how this performance can be optimized using the same tool.

2.1. Proposed Materials

This section investigates the different materials used in synthesizing the suggested novel membrane. It addresses their chemical structure, their physical and chemical properties, in addition to their applications. These materials are:

- Polyaniline (PANI)
- Zirconium phosphate (ZrP)
- Ionic liquids (ILs)

2.1.1. Polyaniline. Polyaniline (PANI) is conjugated polymer directly driven from aniline ($C_6H_5NH_2$). While the polymer can be prepared electrochemically from aniline; without any admixtures via potentiostatic, potentiodynamic and galvanostatic approaches, it is usually prepared chemically via oxidation [18]. Variety of oxidants can be used for PANI preparation such as persulfates and dichromates. Among all, ammonium persulfate is the most widely used oxidant, by which PANI shows a 90% yield as well as a high conductivity of 10^{-1} S/cm [19]. The two-step chemical polymerization of PANI is shown in Figure 3.

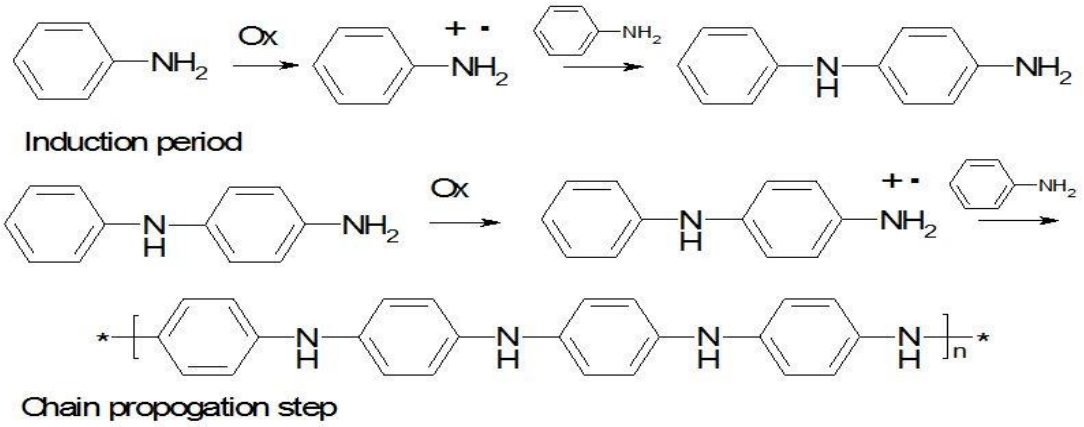

Figure 3: Polymerization mechanism of aniline to polyaniline (PANI) [19].

In addition, PANI is also prepared in the presence of a dopant, an acid or a base, depending on the desired application [19]. Conductive polyaniline, commonly known as emeraldine salt (ES), is synthesized doped in acidic medium (pH 1-3) [19]. The typical ionic conductivity of PANI-ES is around 1S/cm [20]. Depending on the degree of doping, the conductivity of PANI as well as other properties such as thermal stability, density and hydrophilicity can vary [20]. An alternative non-conductive polyaniline known as emeraldine base (PANI-EB) can be formed in case of exposure of PANI-ES to an alkaline medium. However, this polymer can be brought back to its conductive form via re-protonation (usually with H_3PO_4) as presented in Figure 4 [20].

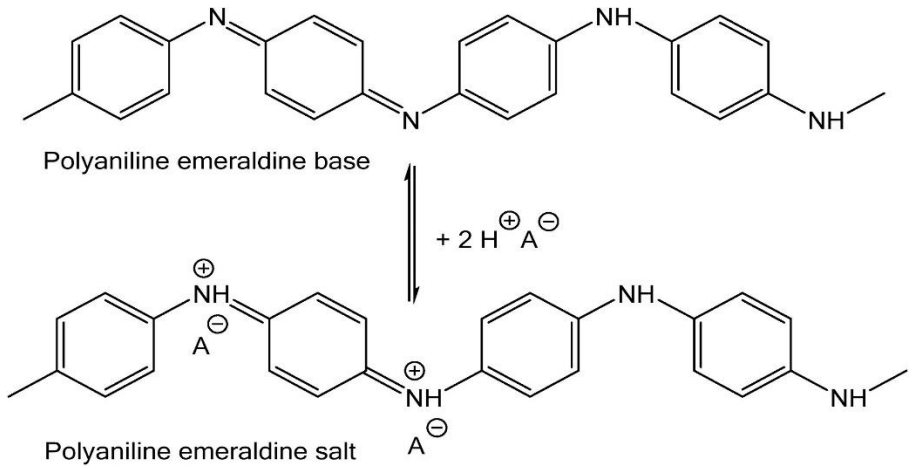

Figure 4: Re-protonation of PANI-EB to PANI-ES [20].

In general, PANI is has very simple doping/de-doping chemistry (easy to synthesize), great ion- exchange characteristics, high specific capacitance, good electrical properties, excellent thermal stability and has low cost of intention [21]. In addition to its high ionic conductivity mentioned earlier, the electrical conductivity of PANI can be as high as 1.2×10^3 S/cm due to the high van der waals interactions between benzene and quoined PANI rings [22, 23]. The high electron conductivity of PANI allows it to be implemented in electrical applications such as rechargeable batteries and organic transistors [23].

Furthermore, PANI can be used for antistatic and anticorrosion coatings, sensors and separation membranes [24]. Unfortunately, a major drawback of conducting polymers is that they present weak mechanical properties [25]. However, the high flexibility of PANI allows it to combine easily with other materials. The availability of abundant N-sites as well as the unique conjugated structure allows PANI to bond and couple with other materials such as carbonaceous materials, metal compounds or other polymers; allowing the resultant composite to have superior properties due to synergistic effects [26]. As a matter of fact, in this proposal, PANI will be coupled with ionic liquids (ILs) to improve the conductivity.

2.1.2. Zirconium phosphate. The inorganic zirconium hydrogen phosphate (ZrP), which originally has the chemical formula of $Zr(HPO_4)_2$, was proven to be a potential conducting material for membranes used in fuel cells [27]. Considering the weak acidic group and its layered structure, the protons from the POH group can transfer freely and be exchanged with other ions [28]. In addition, it was established that ZrP can be refluxed in water for few weeks and withstand any structure breakdown [29]. This is mostly due to its high mechanical stability. ZrP also displays excellent thermal stability. A thermo-gravimetric analysis (TGA) showed that only less than 10% weight loss of crystalline form of ZrP (α-ZrP) was observed up to 800 ^oC as shown in Figure 5 [30].

Alongside its stability, the foundation of α-ZrP which was done by Li et al. [31], resulted in an enhanced proton transfer properties and encouraged utilizing the material into PEMFCs. The α-ZrP can be prepared via direct precipitation of zirconium salt with

phosphoric acid; in the presence of a complexing agent (i.e. hydrofluoric acid, oxalic acid, etc.) [32]. The synthesis time of crystalline ZrP may take up to weeks in order to achieve high degree of crystallinity. The synthesis of α-ZrP paved the way for the development of alternative forms of crystalline ZrP such as $Zr(HPO_4)_2$ or τ-ZrP, $ZrPO_4(H_2PO_4 \cdot 2H_2O$ or γ-ZrP, and $Zr(HPO_4)_2 \cdot 6H_2O$ or θ-ZrP [33].

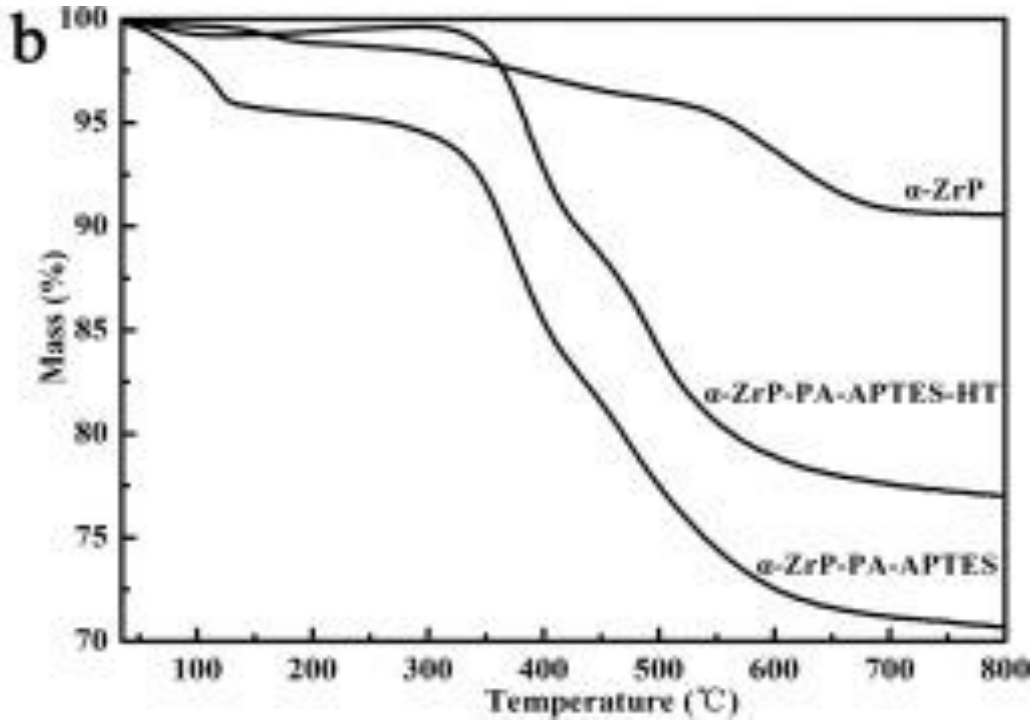

Figure 5: TGA result for different forms of α-ZrP [30].

2.1.3. Ionic liquids. Ionic liquids (ILs) are organic salts that can maintain their liquid phase at room temperature. They are highly nonvolatile, nonflammable, thermally and electrochemically stable and have remarkable ionic conductivity (10^{-2}-10^{-4} S/cm) even at low humidity conditions [34]. Chemically, unlike ionic solutions, ionic liquids are formulated entirely from ions and do not contain solvents as illustrated in Figure 6 [34]. The presence of these ions in the chemical structure of ILs enhances their abilities of meeting the desired properties for most electrochemical applications. Figure 7 presents the most widely used ILs' ions; where imidazolium-based ILs are the most widely studied.

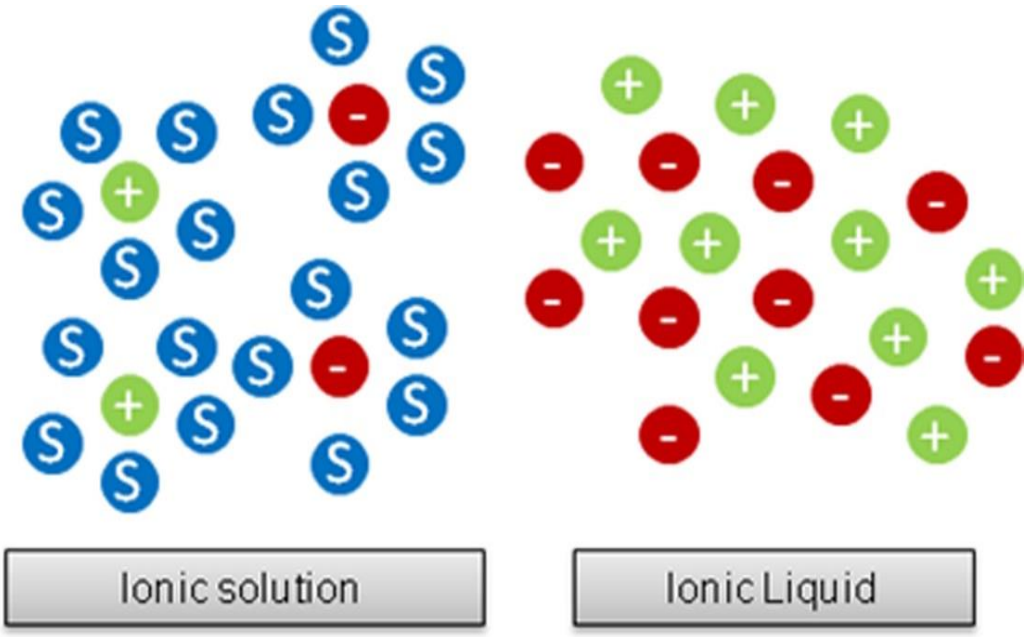

Figure 6: Chemical structure of ionic liquid vs. ionic solution [34].

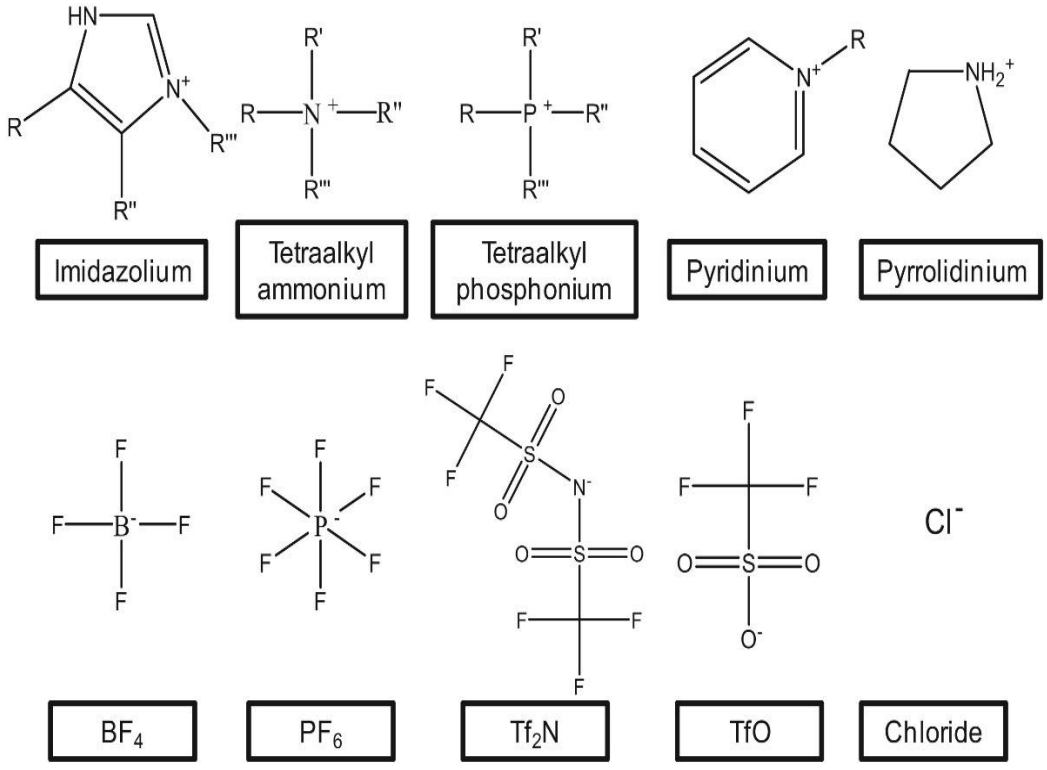

Figure 7: Different ionic groups used in ionic liquids [34].

There are two major types of ILs: aprotic and protic. The first type is generally suitable for lithium batteries due to its high mobility and ions concentration. On the other hand, protic ILs have active protons located on cations [35]. This implies their applicability as electrolytes in fuel cells. Furthermore, due to their independency of water content, protic ILs can operate in cells at elevated temperatures (above 100^{o}C) [35]. ILs are obtained based on the Brønsted acid/base neutralization reaction shown below.

$$HA+B \rightarrow \leftarrow BH^{+} + A^{-}$$

2.2. High Temperature Membranes

The high temperature operation in proton exchange fuel cells offer several attractive characteristics as mentioned previously in this context. Hence, there is an incentive to develop alternatives for the current low temperature membrane (Nafion). The development of high temperature membranes for PEM fuel cells was addressed intensively in the literature [32 - 44]. This section will address some of the most common high temperature based membranes, which are:

- Polybenzimedazole (PBI) doped with phosphoric acid based membranes.
- Sulfonated poly-ether-ether-ketone (SPEEK) based membranes.
- Cellulose/poly-aryl-ether-ketones (SFPAEKs) based membranes.

More specifically, this section focuses on the development of membranes based on the materials used in this thesis work. It discusses conductivity results for individual membranes, as well as conductivity results of their combination where applicable. These membranes were also fairly discussed in literature [45 - 57] and they can be summarized as follows:

- PANI based membranes
- ZrP based membranes
- Ionic liquid membranes
- Composite membranes

2.1.1. PBI based membranes. PBI represents a large family of aromatic heterocyclic polymers containing benzimidazole units [36]. It was first utilized in high

temperature proton exchange membranes (HTPEMs) in 1995 by Wainright [37]. PBI based membranes have low gas permeability, mechanically stable, and conductive even at high temperatures [38]. In return, they have high glass temperature (425-435 ^{o}C), which makes the material almost insoluble in inorganic solvents [39]. Another drawback of PBI (usually prepared while doped in phosphoric acid) is that its mechanical strength degrades with higher doping levels as the acid turns to leach out from the membrane [40].

In 2017, Xue Tian and co-workers [41] studied the conductivity and the mechanical properties of a PBI-based membrane. They used PBI doped in 85% phosphoric acid and improved its structure by doping it in ionic liquid (IL) in order to improve the thermal stability and reduce the mechanical degradation. The results showed excellent proton conductivity at elevated temperatures with a maximum value of 0.061 S/cm (for 15% wt. of IL) obtained at 180^{o}C as shown in Figure 8 [41]. The results were also compared with a PBI membrane (without ionic liquid) which was found to be much lower with a value of 0.025 S/cm at the same temperature.

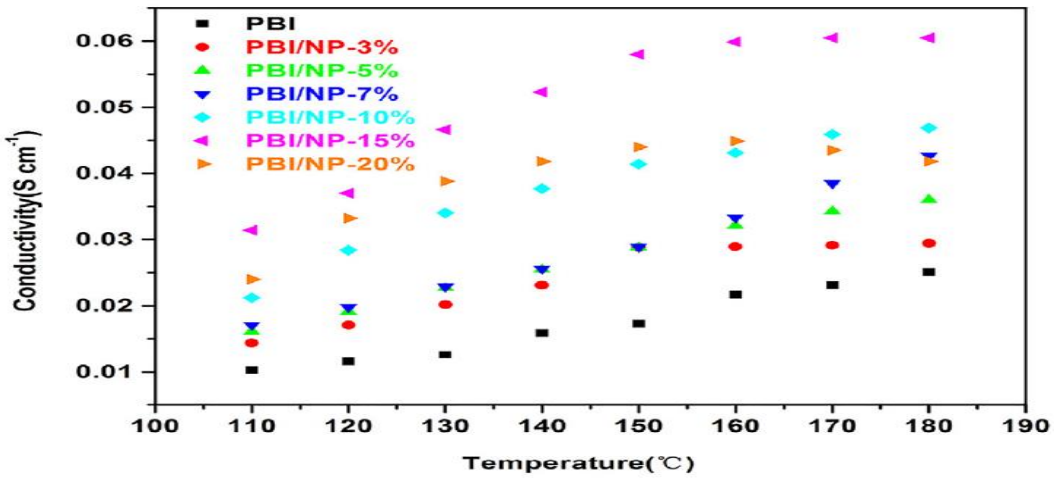

Figure 8: Conductivity of PBI/IL membranes at high temperatures [40].

The results of Tian perfectly agree with that of Bao, Zhang and Liu [42] who also fabricated a PBI-IL based membrane. In fact, Bao and his fellows succeeded to reach a higher temperature of 220 ^{o}C in which they found the conductivity to be the maximum with

a value of 0.04 S/cm [42]. They concluded that the addition of IL enhances the mechanical properties remarkably. A 90% increase in ultimate tensile strength was obtained with a 40% rising in Young's modulus as well compared to pure PBI membrane [42].

Another recent study (2018) by Muthuraja et al. [43] also showed great conductivity results. However, in this study they synthesized a nano-fiber material based on PBI called poly (aryl sulfone ether benzimidazole) (SO2-OPBI). The synthesized material is thermally stable up to 160^{o}C where it represents a peak of 0.0667 S/cm in proton conductivity [43].

2.1.2. SPEEK based membranes. The hydrocarbon polymer, SPEEK, is considered to be very effective in PEMFCs applications. The great thermal and mechanical stabilities, along with the high proton conductivity of the material (depending on the sulfonation degree), ensure the possibility of utilizing the material in HT-PEMFCs [44]. In 2013, Iulianelli et al. [45] presented their work on SPEEK merged with cardo group (SPEEK-WC). Conductivity results were very promising up to 120^{o}C. The maximum proton conductivity reached a value of approximately 0.067 S/cm at 120^{o}C [45].

Better results were obtained later in 2016 by Song et al. [46], where they synthesized a SPEEK-PBI based membrane. Conductivity measurements showed a very high conductivity of 0.099 S/cm at an optimum temperature of 180^{o}C and a relative humidity of 50% [46]. This result perfectly coincides with that of commercial Nafion membranes at low temperatures. In fact, the conductivity of SPEEK/PBI (20 wt. %) reached a value of 0.198 S/cm at 170^{o}C under fully humidified conditions [46].

2.1.3. Cellulose/SFPAEKs membranes. Cellulose is usually blended with another polymer in order to be used as a PEM. As a matter of fact, cellulose is believed to be a strong additive to polymers since it improves variety of their mechanical properties [47]. The material is abundant in nature and its extraction from plants can be easily done. Nanocrystalline cellulose (NCC) is widely used in PEMFCs applications due to its high surface area, remarkable crystal structure and its superior mechanical properties [48]. In 2016, an intensive study conducted on NCC blended with sulfonated poly-aryl-ether-ketones (SFPAEKs) presented promising results. A remarkable proton conductivity of 0.234 S/cm obtained at 100^{o}C [48]. Moreover, the study displayed a noticeable

improvement in the mechanical properties of the hybrid membrane compared to pure SFPAEK.

2.2.1. PANI based membranes. The excellent properties of PANI allow it to be used as a separator membrane as discussed earlier. Various studies have been conducted; investigating the possibility of using PANI in a PEMFC [48 - 53]. In 2008, Yang and co-workers [49] examined the conductivity of acid-doped meta-polyaniline (m-PANI) at elevated temperatures. The experimental results showed a reasonable proton conductivity of approximately 0.002 S/cm at a maximum temperature of 120 ^{o}C [49]. A major problem of this work was the observed color change and flexibility loss of the membrane, which indicates shrinkage in the mechanical stability in the long term. Therefore, as mentioned even in the previous section, PANI must be coupled with another material in order to overcome the mechanical stability problem and enhance its properties in general.

The combination of PANI and other materials is expected to increase the conductivity and improve the mechanical properties. Zhao et al. [50] investigated the conductivity of PANI coupled with sulfonated poly-arylene-ether-ketone bearing carboxyl groups (SPAEK-C). It was found that proton conductivity can be as high as 0.093 and 0.24 S/cm at 25 ^{o}C and 80^{o}C respectively [50]. A recent work developed by Sun and co-workers [51] in 2017 presented better results. Sun and his colleagues synthesized a sulfonated PANI-PBI composite membrane, which displayed an excellent conductivity of 0.13 S/cm at fully hydrated conditions and 0.064 S/cm at anhydrous medium [51]. These results were obtained at an elevated temperature of 180 ^{o}C.

A study by Stejskal, et al. [52] demonstrated superior conductivity measurements. They investigated a new material synthesized by merging PANI with an ionic liquid (IL) known as 1-ethyl-3-methylimidazolium trifluoromethane-sulfonate. Although the purpose of the study was not to develop PEMFC membranes, the obtained proton conductivity was as high as 0.43 S/cm [52]. This study indeed sheds the light on ILs and how they can be engaged with PANI for fuel cells applications.

Many approaches were followed in the literature to enhance Nafion's performance at higher temperature by the introduction of other polymers. Polyaniline (PANI) is one

example. Escudero-Cid et al. [53] synthesized a Nafion 117-PANI membrane for DMFC's applications. The objective of the study was to enhance proton conductivity and decrease the permeability of methanol into the membrane. The penetration of methanol into the membrane poisons the cathode and kills the electric circuit [53]. Results showed a noticeable decrease in methanol permeability from 2.55×10^{-6} to 2.08×10^{-7} cm^2/s. No improvement on proton conductivity was reported.

Yang et al. [54] reported an actual increase in proton conductivity using Nafion112-PANI composite material. Different samples of Nafion 112-PANI membranes were prepared at different reaction times (1-4 hours). The results showed a better conductivity of the hybrid material compared to the pure Nafion 12 as shown in Figure 9 [54]. Furthermore, degradation of the cell performance was noticed in both; pure Nafion cell and the composite cell; however, it was slower in the composite case as displayed in Figure 10 [54]. Therefore, the study concluded that Nafion-PANI membranes are very promising at low humidity conditions.

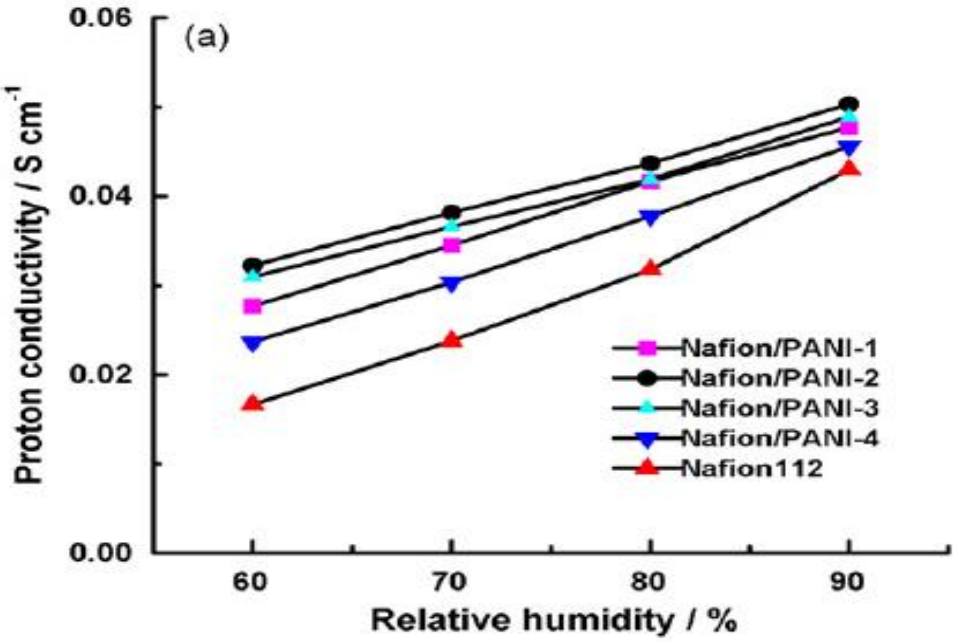

Figure 9: Conductivity at various humidity conditions for Nafion/PANI membranes at 30°C [54].

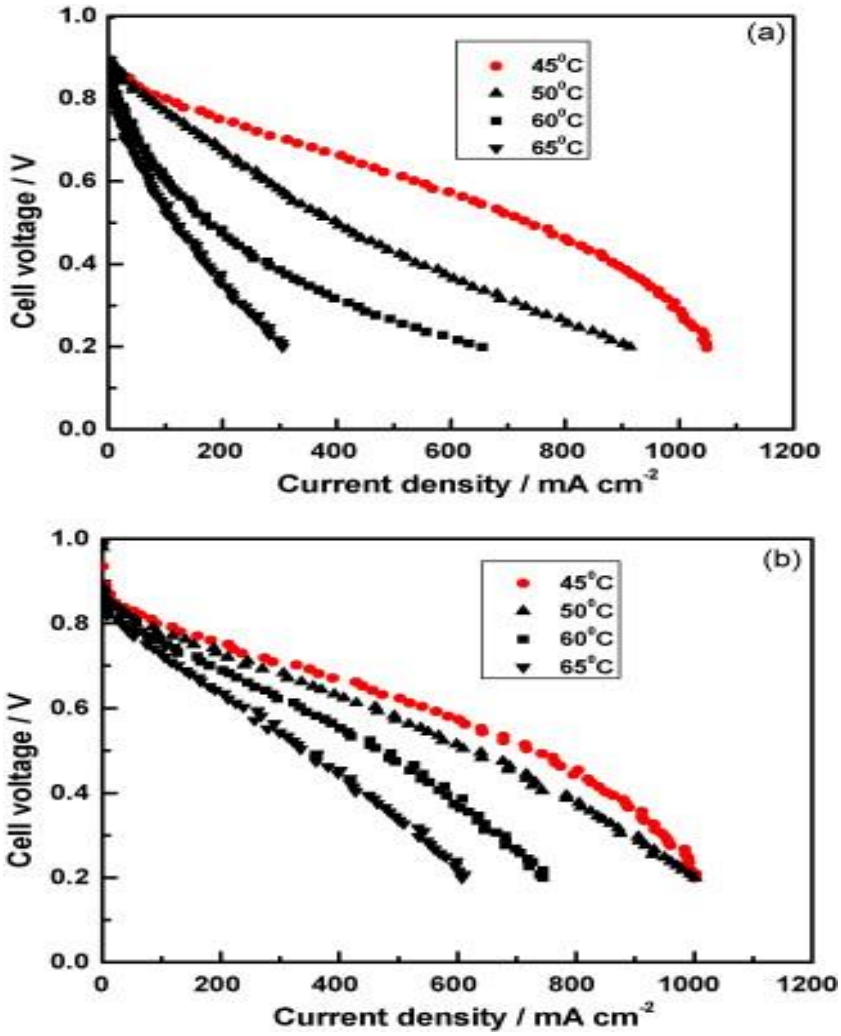

Figure 10: Polarization curves for Nafion (a) and Nafion/PANI (b) composite membranes [54].

2.2.2. ZrP based membranes. Inorganic compounds such as zirconium phosphate (ZrP) have been intensively studied in literature to support Nafion based membranes at high temperatures [55]. ZrP has high thermal stability; which suggests its high functionality at elevated temperatures. ZrP fabricated over polytetrafluoroethlyne (PTFE) sheets had a reasonable ionic conductivity in the order of 10^{-2} S/cm at high temperatures[56] . The thermal stability of Nafion membrane by the addition of ZrP was implemented in many studies. For instance, in 2001, Yang et al. established a Nafion/Zrp membrane that is thermally stable up to 150 ^{o}C [57].

Furthermore, although the conductivity of ZrP is lower than pure Nafion, a recent study by Ozden et al. [58] suggested that their combination leads to higher conductivity results than pure Nafion. The study showed that Nafion with 5% ZrP membrane exhibited a conductivity of 0.223 S/cm at 80 ºC compared to 0.123 S/cm for pure Nafion. The composite membranes also showed higher power densities, more endurance for fuel crossover and enhanced water-uptake and thermal stability [58]. Table 1 presents a summary of the main foundlings of the study.

Table 1: Summary of the main results for Nafion/ZrP membranes [58].

Membrane type	**Activation energy (kJ/mol)**	**Water uptake (%)**	**Proton conductivity (S/cm)**				
			25 ºC	**50ºC**	**60ºC**	**70ºC**	**80ºC**
Nafion 115	10.7	10.1	0.081	0.107	0.119	0.129	0.132
N- 2.5% ZrP	15.4	11	0.101	0.175	0.206	0.213	0.218
N- 5% ZrP	19.5	13.3	0.078	0.140	0.172	0.198	0.223

2.2.3. Ionic liquid based membranes. Recently, intensive studies have been conducted regarding polymer-ionic liquid based membranes. Mixing the two materials presented a noticeable enhancement in the degree of ion dissociation, improved the

concentration of ionic moieties and modified the glass temperature of the material [59]. Accordingly, the transport properties of the new developed material are modified. Table 2 presents different studies that report the conductivity of polymer-ionic liquid membranes. Nevertheless, Stejskal et al. reported better conductivity results when using a PANI-IL combination as mentioned earlier. Therefore, in this work, it is believed that synthesizing a PANI-IL membrane would give remarkable conductivity results.

Table 2: Conductivity measurements for some polymer-ionic liquid based membranes [58].

Ionic liquid/polymer type	**Conductivity (S/cm)**	**Notes**
$EMImTf_2N/TMOS/PO(OCH_3)_3$	0.0054 at 150°C	High chemical and thermal stability and high power density
$MPnTf_2N$-$MPzTf_2N$-$MPyTf_2N$-$MImTf_2N$-$EInTf_2N$/PVdF	0.01 at 140 °C	Thermally stable
$BMImBF_4$/SPEEK	0.0104 at 170°C	Conductive due to ionic cluster
$BMImPF_6$/MMA	0.0002	Flexible and transparent
EMPyr(FH)F/HEMA	0.0819 at 100°C	Performance decreases beyond 80°C
$TMPA^+$/Nafion Cl^-; DTA^+ Cl^-; CTA^+ Br^-; $BMIm^+$ $PF6^-$; OMIm $PF6^-$	4×10^{-6} Nafion/DTA^+ 4×10^{-5} Nafion/CTA^+	-

2.2.4. Composite membranes. The combination of PANI with IL was proven to increase the ionic conductivity of the membrane. A study conducted by Rogalsky et al. [60] showed that the ionic conductivity of a PANI membrane was increased from 0.00045 to 0.004 S/cm by the addition of IL at 180 ^{o}C. The study also concluded that the combination of PANI and protic ionic liquids can be considered as a more cost effective membrane solution for an anhydrous high temperature fuel cells applications [60].

The integration of zirconium phosphate with ionic liquids also result in a noticeable increase in proton conductivity. According to Al Othman et al. [61], when introducing IL to a ZrP/glycerol composite membrane, the conductivity was enhanced from 0.02 to 0.061 S/cm at 200 ^{o}C and waterless conditions. The increase in proton conductivity was due to the interaction between the 3 components, which allowed a formation of multiple hydrogen bonds; providing free pathway for proton transfer [61].

Therefore, it was believed that synthesizing a membrane combining all three materials (PANI, ZrP and IL) mentioned above would result in a conductive polymer electrolyte membrane that can be used for high temperature fuel cells processes. The synthesized membrane is also believed to be thermally and mechanically stable and can solve the dehydration problem of a Nafion membrane at high temperatures. The mechanism of how the membrane was synthesized along with electrical performance of the membrane is also to be discussed later in this work.

2.3. Factorial Design in Fuel Cells:

The modelling of fuel cells using factorial design (FD) has received a considerable attention in literature. Scientists often use this approach to determine the key factors that affect a certain response within the fuel cell. The response is usually conductivity or current density; which are the main factors of interest in all types of fuel cells. The modelling can be accomplished using either Minitab, ANOVA or any statistical software. Statistical date are provided with the model; suggesting wither the model was successful or not.

Endoo et al. [62], performed a FD modelling in order to identify key variables in membrane electrode preparation in PEMFCs. The generated model studied the effect of PTFE quantities, drying temperature, drying density and dry atmosphere on the current

density of the cell as can be seen from Table 3. Results showed that the drying temperature and the dry atmosphere as well as their interaction together were the main factors affecting the cell performance in the model.

Identifying the important factors can be done by looking at their corresponding P-values. The P-value represents the probability of obtaining results as extreme as the actual; keeping in mind that the null hypothesis is valid [63]. The null hypothesis states that for a population, there is no difference in certain properties [63]. In practice, a significance level (α) must be determined in advance. The lower the P-value than the significance level suggests that there is no enough evidence to reject the null hypothesis and that the model is valid [63].

Therefore, in Endoo's model, the P-values were sufficiently low as can be shown from Table 4. This suggests the adequacy of his model. The model concluded that at a fixed potential of 0.6 V, current density (i) can be determined through the following linear equation (Equation 1):

$$i = 50.02 - 15.43B - 8.45D + 7.48BD \quad (1)$$

where B and D are the drying temperature and the dry atmosphere factors respectively.

Table 3: Endoo et al. [62] parameters and its response on current density.

Run no.	**A**	**B**	**C**	**D**	**Current density (mA cm^{-2})**	**Variable**	**(−)**	**(+)**
1.	−	−	−	−	85.0	A = quantity of PTFE (μL)	0	10
2.	+	−	−	−	82.9	B = drying temperature (°C)	140	300
3.	−	+	−	−	39.9	C = drying time (h)	0.5	1
4.	+	+	−	−	33.8	D = dry atmosphere (air/N_2)	Air	N_2
5.	−	−	+	−	67.9			
6.	+	−	+	−	91.2			

7.	−	+	+	−	23.0
8.	+	+	+	−	44.2
9.	−	−	−	+	40.4
10.	+	−	−	+	55.7
11.	−	+	−	+	49.3
12.	+	+	−	+	28.3
13.	−	−	+	+	67.9
14.	+	−	+	+	32.7
15.	−	+	+	+	21.2
16.	+	+	+	+	37.0

Table 4: Endoo et.al model statistical results [62].

Sources of variability	**Sum of square**	**DF**	**Mean square**	***F*-value**	**Probe > F**
Model	6889.08	5	1377.8	10.87	0.0009
B	3810.90	1	3810.48	30.07	0.0003
D	1143.62	1	1143.31	9.02	0.0133
BD	984.92	1	984.26	7.76	0.0192
ABC	494.28	1	494.28	3.90	0.0765
ABCD	456.36	1	456.36	3.60	0.0870
Residual	1267.54	10	126.75		
Total	7662.35	15			

Factorial design can also be used for optimizing fuel cells performance. Dante et al. [64] succeeded to optimize a H_2/O_2 PEMFC following ANOVA FD modelling. The model analyzed four different factors to come up with optimum operating conditions of the cell. The tweaked factors where the hydrogen and oxygen pressures (PH_2 and PO_2) in

addition to their flow rates (QH_2 and QO_2). The model studied the effect of each of these factors on the output power of the cell. The initial two-levels of each factor is shown in Table 5. Following the optimization of the results as shown in Figure 11, the new operating conditions of the cell were PH_2: 69:0 kPa, PO_2: 138:0 kPa, QH_2: 4.1×10^{-5} m^3/s, and QO_2:1.2×10^{-4} m^3/s.

Table 5: Dante et al. [64] FD factors and their effect on cell potential and current intensity.

Effects	**PH_2**		**PO_2**		**QH_2**		**QO_2**	
Upper/ lower Levels	169.0 kPa	96.5 kPa	172 kPa	276 kPa	4.1×10^{-5} m^3/s	8.25×10^{-5} m^3/s	4.1×10^{-5} m^3/s	8.2×10^{-5} m^3/s
Potential (V)	0.234		−0.299		−0.276		0.503	
Current intensity (A)	0.138		−0.410		−0.370		0.547	

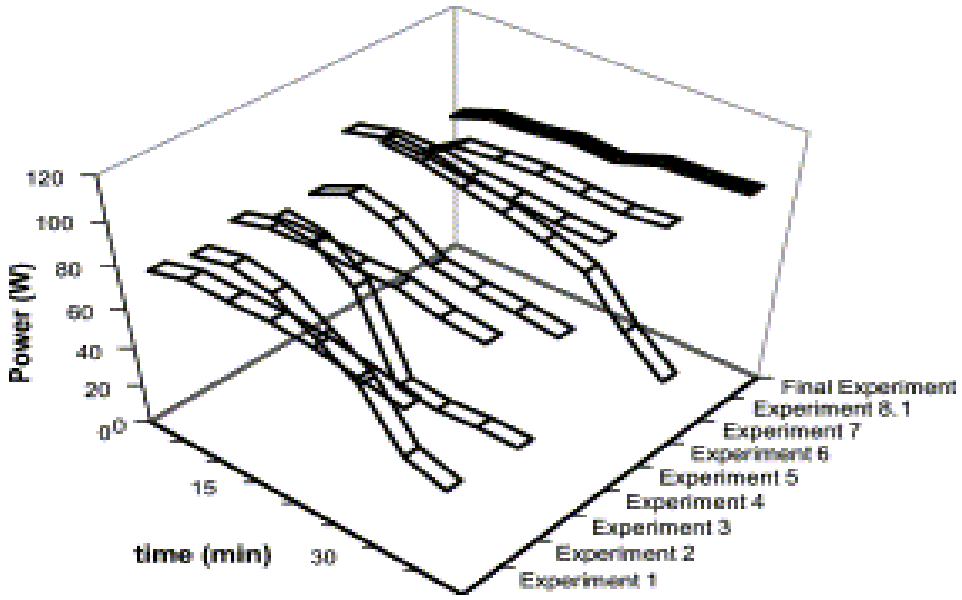

Figure 11: Dante et al. [64] FD model to optimize the cell performance.

In addition, a more complex approach can be used in FD modelling; which is using 3-level FD instead of the regular 2-level models. In this model, 3 points are used to run the analysis instead of two. In 2012, Cheng and co-workers [65] investigated the effects of certain operating factors on the fuel cell performance using a 3-level FD approach. The studied factors were the bipolar flow channel design, operational temperature and the relative humidity as shown in Table 6 below.

Table 6: Cheng et al. [65] 3-level FD factors.

Factors	**Symbol**	**Level 1**	**Level 2**	**Level 3**
Channel pattern	A	Parallel-I	Parallel-II	Parallel-III
Relative humidity of cathode	B	50%	75%	100%
Operating temperature (K)	C	333	343	353

The model provided statistical results in addition to main effect and interaction results. The statistical results were mainly related to the model linear regression and the normality of the model. As illustrated in Figure 12, the model was proven to be linear from the linear probability curve (Figure a) and also the points were normally distributed as can be viewed from the observation order plot (Figure b).

When it came to the main effect results, it was clear that the channel pattern has a significant effect on the power density output followed by the operating temperature; where the relative humidity was noticed to be insignificant as shown in Figure 13. Where for the interaction effect results, no clear interaction was observed between channel pattern and relative humidity or relative humidity and operating temperature as shown in Figure 14. The only apparent interaction was noticed to be between channel pattern and operating

temperature (Figure C). When temperature is increased and channel pattern III is used, more power density is obtained.

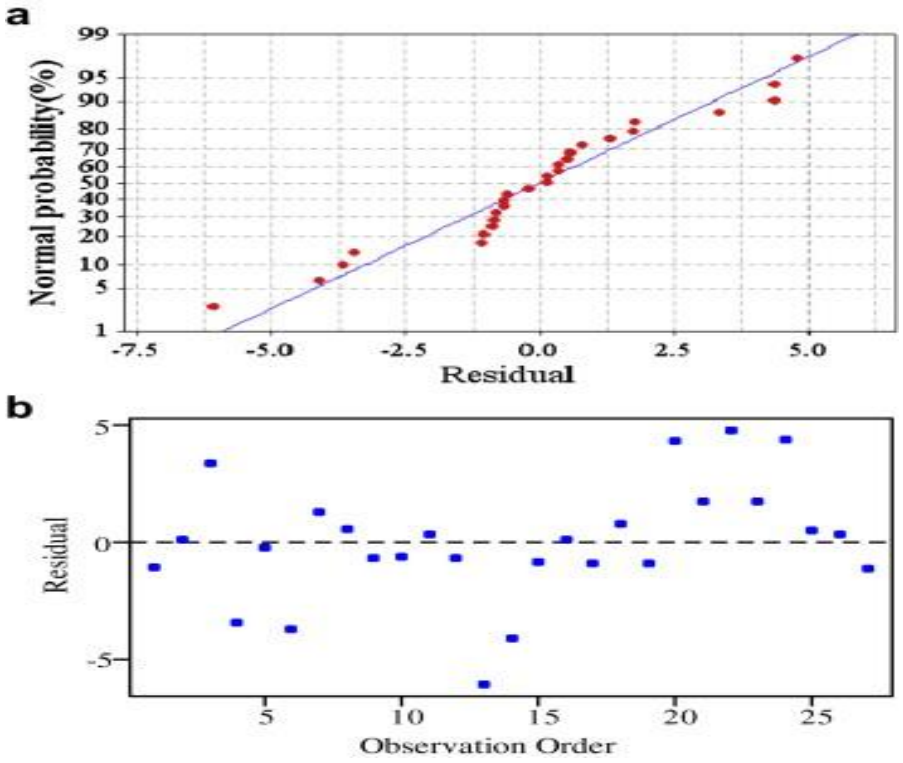

Figure 12: Normal probability (a) and observation order (b) curves for Cheng et al. [65] model.

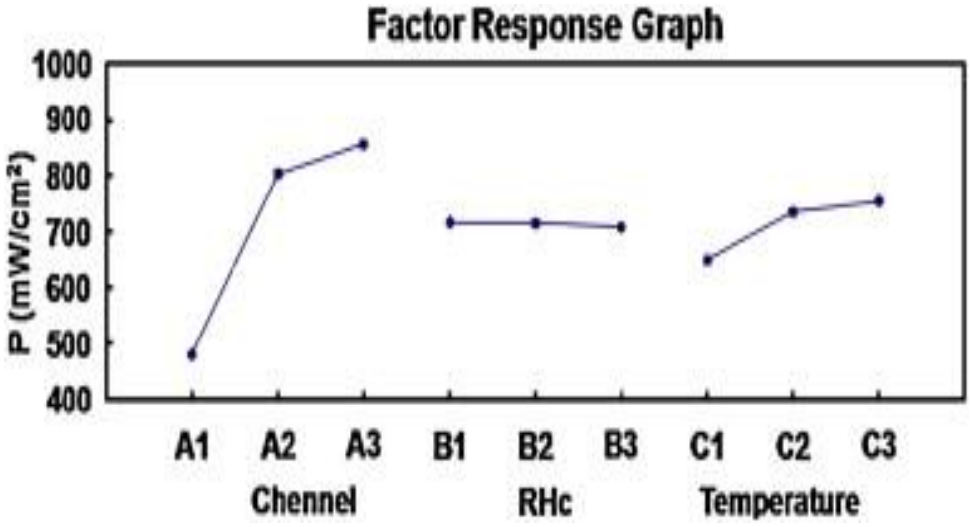

Figure 13: Main effect results for Cheng et al. [65] FD model.

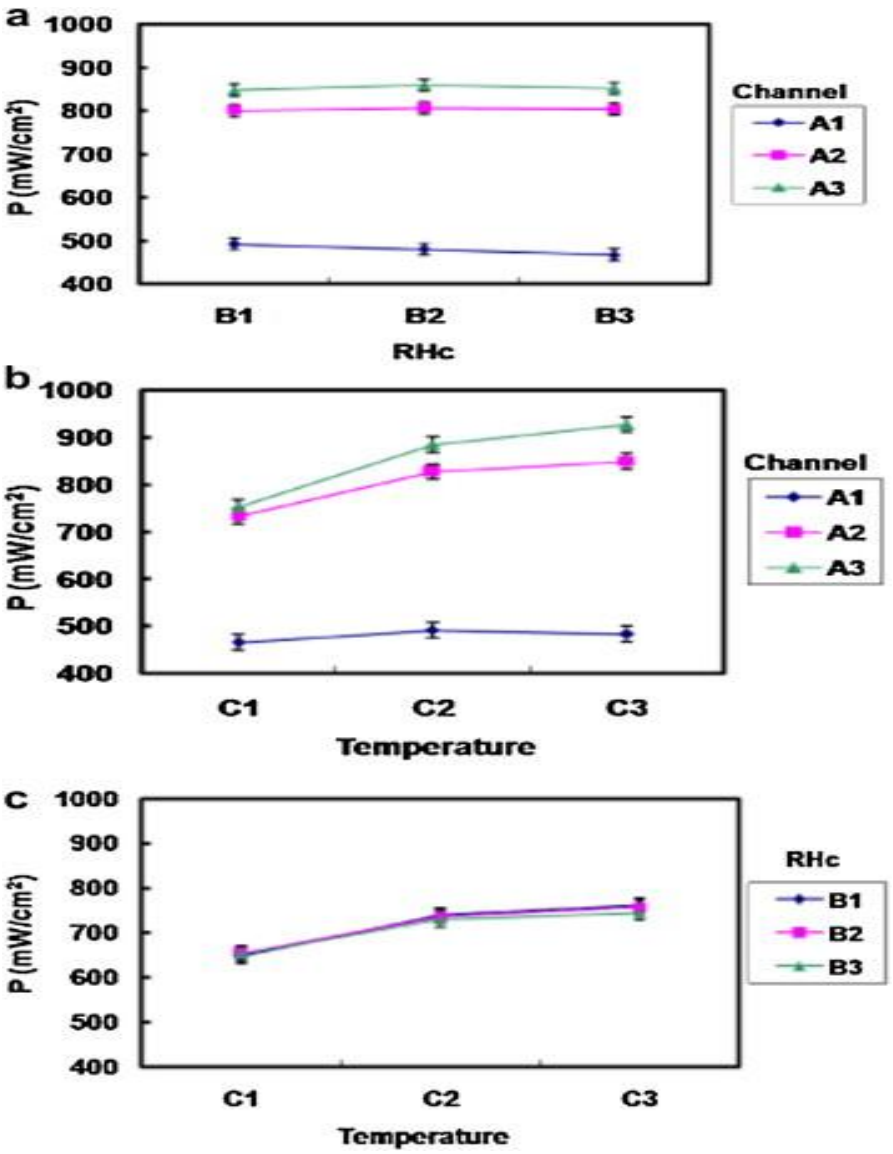

Figure 14: Interaction effect results for Cheng et al. [65] FD model.

Unfortunately, all studies mentioned earlier where conducted using Nafion membranes. In addition, all previous models were concerned with the cell performance (power densities and current densities) instead of the membrane conductivity. Therefore, this thesis work will focus on developing a FD model based on Nafion-free membranes. The developed model will also target the proton conductivity as the response output variable instead of power or current densities. The cell performance will eventually be predicted using a theoretical approach based on the experimental conductivity values.

Chapter 3. Experimental Plan and Methodology

The thesis work is divided into two major parts. The first part aimed at developing a novel polymer electrolyte membrane (PEM) for fuel cells applications at elevated temperatures (~ 180 °C). The second part focused on modelling the synthesized membranes using FD in order to identify the key factors affecting the performance of the fuel cell.

The synthesized membrane should obey certain criteria. It should have high proton conductivity at low humidity conditions and elevated temperatures. It should also be thermally and mechanically stable; in other words, it should be highly non-degradable and have long durability.

Generally, this membrane should be synthesized at a lower cost than that of Nafion's. Hence, a new PEM was synthesized based on polyaniline (PANI), zirconium phosphate (ZrP) and ionic liquids (IL). To ensure the mechanical integrity required in a fuel cell membrane is intact, polytetrafluoroethylene (PTFE) was used as a supporting material.

PANI is a very good conducting polymer that shows high thermal stability even at elevated temperatures. Furthermore, the weak acidic groups in ZrP strongly promote proton transfer. Also, protic ILs are known for its hydrophilicity and proton conducting properties. In addition, their incorporation with polymers and ZrP showed remarkable improvement on the composite properties; specially its conductivity as discussed earlier in the work. Finally, PTFE is known for its excellent chemical and thermal stability up to 180^{o}C [66]. Therefore, using the combination above is believed to create a novel conductive membrane that can withstand high temperatures.

In general, this chapter will discuss the experimental work required to develop PANI/ZrP/IL membranes supported on PTFE sheets. After that, it will explain the methodology of how the membranes' conductivity were measured. It will also address a theoretical modeling approach based on statistical factorial design to study the effect of changing certain factors on the membrane conductivity. Finally, the performance of the targeted fuel cells will be analyzed by developing polarization curves.

3.1. Preparation of Polyaniline (PANI)

Polymerization of aniline was done following a modified procedure reported by Youssif et al.[67]. In brief, aniline hydrochloride monomer (0.2M) underwent in situ polymerization via oxidizing with potassium persulfate (KPS). Initially, aniline hydrochloride was dissolved in water and then 200 ml of sodium dodecyl sulphate (SDS) (70:30 mass to mass percent in xylene) was also dissolved in water to form a white (milky) emulsion.

The KPS oxidant (0.074 mols in 40 mL water) was then added to the emulsion and kept under stirring for 1 hour. During the first 5 minutes the emulsion changed color from milky white to brown/orange to dark green and finally black. To ensure complete polymerization, the reaction was kept active for 24 hours. After that, PANI powder was obtained, filtered and washed with water and acetone, and dried in oven at 70 ^{o}C for 24 hours.

3.2. Preparation of Zirconium Phosphate and Ionic Liquids.

ZrP was purchased from Sigma Aldrich (CAS 13772-29-7) and it was used as is without any modifications. ILs were purchased from from IoLiTec GmbH and used without any modification. The two ILs used in this work are:

- 1-Hexyl-3-Methylimidazolium Tricyanomethanide (HMT).
- Diethylmethylammonium Methanesulfonate (DEMM).

3.3. Membrane Synthesis

The membrane synthesis starts with a porous polytetrafluoroethylene (PTFE) purchased from Sterlitech, pore size (0.2 µm) will be used as a support. PTFE was placed in between two Teflon hoops as shown in Figure 15. PANI was prepared using the procedure described earlier then dissolved in 10 mL isopropanol with/without the addition of IL and/ZrP to prepare a solution. The solution then underwent sonication via ultra sound for 5 minutes to ensure proper mixing. This allowed the solution to be absorbed smoothly into the PTFE.

The prepared solution was then poured (1 mL) over the thin PTFE sheet. A hoop was used to ensure that the sheet is straightened enough so that the solution can fill all the

voids in the PTFE. Also, the solution was well distributed over the top and bottom sides of the PTFE. The membrane was then dried in an oven for 24 hours at 90 ^{o}C and then cooled at room temperature for 2 hours. Figure16 views the synthesized membrane.

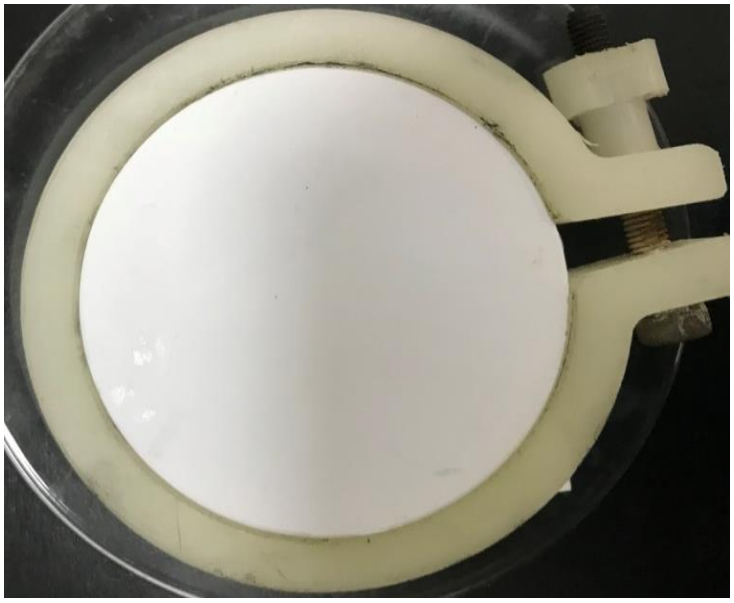

Figure 15: PTFE membrane before adding PANI/IL solution placed on a hoop.

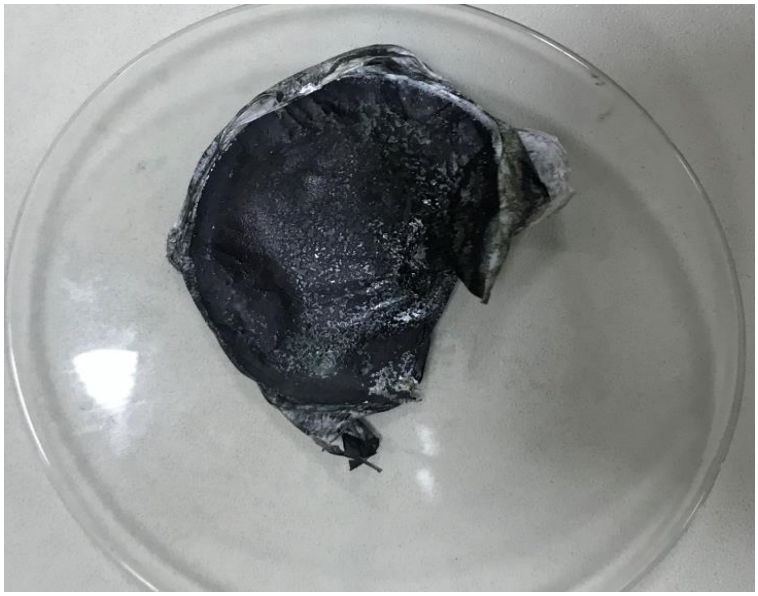

Figure 16: Synthesized PANI/IL membrane supported on a PTFE sheet.

3.4. Factorial Design

In this work, a two-level factorial design was used to analyze the experimental data. The factorial design is a true statistical experiment where multiple factors (independent variables) are varied to study their response on one or more dependent variable(s) [68]. By varying the factors, one may study the effect of each factor on the dependent variable(s) simultaneously as well as their interaction's effect. The "two-level" terminology indicates that each factor should have a low and a high level [69].

The selection of these levels should not be random. In fact, both levels should be numerically close since factorial design models assume linearity in between these levels [70]. According to Montgomery [71], to apply a two-level factorial design with n factors, 2^n experiments will be required for the study. In this study 5 factors will be analyzed:

1) Concentration of PANI (A).
2) Concentration of IL (B).
3) Concentration of ZrP (C).
4) Temperature (D).
5) Type of IL (E)

Analyzing 5 factors means conducting 32 (2^5) experiments. However, due to lack of experimental data, the effect of PANI concentration with the type of Ionic liquid was studied independently. In other words, this would mean conducting two different factorial designs; one with 2 factors (4 experiments) and the other with 4 factors (16 experiments).

To correctly analyze the data, the effect of PANI concentration with the IL type was studied first. Based on the results, the more effective IL type was used in the second factorial design model.

Each experiment was repeated 3 times to ensure the validity of the results. This would mean running 12 and 48 experiments respectively. In each factorial design, experiments were run in a random order to eliminate and reduce any bias results. Randomizing the runs would also give strong estimates about the variations by changing any factor and would result in a stronger statistical conclusion.

In addition, each factor should be varied slower than the one before it. Hence, factor B is varied slower than A, factor C slower than B and so on. The interaction between the variables and how fast or slow it varies can be determined through the factorial design matrices displayed in Tables 7 and 8. The interaction variance speed depends on the product (multiplication) of the individual factors.

The 1st factorial design generates a linear regression equation that takes the form of Equation 2 below:

$$y = \alpha_o + \alpha_1 x_A + \alpha_2 x_E + \alpha_{12} x_A x_E \tag{2}$$

where α_o is the average conductivity in all runs of the 1st factorial design.

α_1 represents the single effect of PANI concentration. It can be found from the average of the obtained values from multiplying the column of the conductivity by A column of the 1st factorial design.

α_2 represents the single effect of IL type. It can be found from the average of the obtained values from multiplying the column of the conductivity by E column.

α_{12} represents the cross effect of A and E. It can be found from the average of the obtained values from multiplying the conductivity column by AE column.

x_A and x_E are coded variables (usually between -1 and 1) and they can be found from Table 7. In addition, the relationships between coded variables and the actual factors are given by the expressions in Equation 3 and Equation 4 below:

$$x_A = \frac{PANI\ wt\% - \left(\frac{PANI\ wt\%_{high} + PANI\ wt\%_{Low}}{2}\right)}{\frac{PANI\ wt\%_{high} - PANI\ wt\%_{Low}}{2}} \tag{3}$$

$$x_E = \frac{IL\ type - \left(\frac{IL_{high} + IL_{Low}}{2}\right)}{\frac{IL_{high} - IL_{Low}}{2}} \tag{4}$$

Table 7: Coded matrix for the 1st FD.

Run	x_A	x_E	$x_A x_E$
1	-1	-1	1
2	1	-1	-1
3	-1	1	-1
4	1	1	1

After implementing the design, the chosen IL type is varied in concentration and integrated into the 2nd factorial design which takes the form of Equation 5:

$$y = \beta_o + \beta_1 x_A + \beta_2 x_B + \beta_{12} x_A x_B + \beta_3 x_C + \beta_{13} x_A x_C + \beta_{23} x_B x_C + \beta_{123} x_A x_B x_C + \beta_4 x_D + \beta_{14} x_A x_D + \beta_{24} x_B x_D + \beta_{34} x_C x_D + \beta_{124} x_A x_B x_D + \beta_{134} x_A x_C x_D + \beta_{234} x_B x_C x_D + \beta_{1234} x_A x_B x_C x_D \quad (5)$$

where βo is the average conductivity in all runs of the 2nd factorial design.

β_1 represents the single effect of PANI concentration. It can be found from the average of the obtained values from multiplying the column of the conductivity by A column of the 2nd factorial design.

β_2 represents the single effect of IL concentration. It can be found from the average of the obtained values from multiplying the column of the conductivity by B column.

β_{12} represents the cross effect of A and B. It can be found from the average of the obtained values from multiplying the conductivity column by AB column.

β_3 represents the single effect of ZrP concentration. It can be found from the average of the obtained values from multiplying the column of the conductivity by C column.

β_{13} represents the cross effect of A and C. It can be found from the average of the obtained values from multiplying the conductivity column by AC column.

β_{23} represents the cross effect of B and C. It can be found from the average of the obtained values from multiplying the conductivity column by BC column.

β_{123} represents the cross effect of A, B and C. It can be found from the average of the obtained values from multiplying the conductivity column by ABC column.

β_4 represents the single effect of temperature. It can be found from the average of the obtained values from multiplying the column of the conductivity by D column.

β_{14} represents the cross effect of A and D. It can be found from the average of the obtained values from multiplying the conductivity column by AD column.

β_{24} represents the cross effect of B and D. It can be found from the average of the obtained values from multiplying the conductivity column by BD column.

β_{34} represents the cross effect of C and D. It can be found from the average of the obtained values from multiplying the conductivity column by CD column.

β_{124} represents the cross effect of A, B and D. It can be found from the average of the obtained values from multiplying the conductivity column by ABD column.

β_{134} represents the cross effect of A, C and D. It can be found from the average of the obtained values from multiplying the conductivity column by ACD column.

β_{234} represents the cross effect of B, C and D. It can be found from the average of the obtained values from multiplying the conductivity column by BCD column.

β_{1234} represents the cross effect of A, B, C and D. It can be found from the average of the obtained values from multiplying the conductivity column by ABCD column.

x_B, x_C and x_D are coded variables (usually between -1 and 1) and they can be found from Table 8. In addition, the relationships between coded variables and the actual factors are given by the following expressions (Equations 6-8):

$$x_B = \frac{IL\ wt\% - \left(\frac{IL\ wt\%_{high} + IL\ wt\%_{Low}}{2}\right)}{\frac{IL\ wt\%_{high} - IL\ wt\%_{Low}}{2}} \quad (6)$$

$$x_C = \frac{ZrP\ wt\% - \left(\frac{ZrP\ wt\%_{high} + ZrP\ wt\%_{Low}}{2}\right)}{\frac{ZrP\ wt\%_{high} - ZrP\ wt\%_{Low}}{2}} \quad (7)$$

$$x_D = \frac{Temperature - \left(\frac{Temperature_{high} + Temperature_{Low}}{2}\right)}{\frac{Temperature_{high} - Temperature_{Low}}{2}} \quad (8)$$

Table 8: Coded matrix for the 2nd FD.

Run	x_A	x_B	x_Ax_B	x_C	x_Ax_C	x_Bx_C	$x_Ax_Bx_C$	x_D
1	-1	-1	1	-1	1	1	-1	-1
2	1	-1	-1	-1	-1	1	1	-1
3	-1	1	-1	-1	1	-1	1	-1
4	1	1	1	-1	-1	-1	-1	-1
5	-1	-1	1	1	-1	-1	1	-1
6	1	-1	-1	1	1	-1	-1	-1
7	-1	1	-1	1	-1	1	-1	-1
8	1	1	1	1	1	1	1	-1
9	-1	-1	1	-1	1	1	-1	1
10	-1	-1	1	-1	1	1	-1	1
11	1	1	1	-1	-1	-1	-1	1
12	-1	1	-1	-1	1	-1	1	1
13	1	-1	-1	1	1	-1	-1	1
14	-1	-1	1	1	-1	-1	1	1
15	1	1	1	1	1	1	1	1
16	-1	1	-1	1	-1	1	-1	1

Run	x_Ax_D	x_Bx_D	x_Cx_D	$x_Ax_Bx_D$	$x_Ax_Cx_D$	$x_Bx_Cx_D$	$x_Ax_Bx_Cx_D$
1	1	1	1	-1	-1	-1	1
2	-1	1	1	1	1	-1	-1
3	1	-1	1	1	-1	1	-1
4	-1	-1	1	-1	1	1	1
5	1	1	-1	-1	1	1	-1
6	-1	1	-1	1	-1	1	1
7	1	-1	-1	1	1	-1	1
8	-1	-1	-1	-1	-1	-1	-1
9	-1	-1	-1	1	1	1	-1
10	-1	-1	-1	1	1	1	-1
11	1	1	-1	1	-1	-1	-1
12	-1	1	-1	-1	1	-1	1
13	1	-1	1	-1	1	-1	-1
14	-1	-1	1	1	-1	-1	1
15	1	1	1	1	1	1	1
16	-1	1	1	-1	-1	1	-1

3.5. Electrochemical Impedance Spectroscopy (EIS).

Electrochemical impedance spectroscopy (EIS) was utilized to determine the ionic conductivity of the membrane samples. EIS is a widely used technique, where an alternating potential provided by a potentiostat is applied to a cell. The samples to be analyzed will be placed in between two stainless steel electrodes (cell) connected to the potentiostat. The response of the alternating potential on the sample will be viewed as plot following Nyquist's behavior; hence relating imaginary resistance to the real resistance. Additionally, frequency plays also a roll in showing the curve response. Sometimes adjusting the frequency helps in viewing the response more clearly.

The shape of the response curve is usually semi-circle; indicating that kinetics of the electro-oxidation reaction are the rate determining step. Having the actual response plotted, extrapolating with the first point of the curve with the x-axis gives the value of the real sample resistance. Accordingly, the conductivity (σ) is calculated using Equation 9:

$$\sigma = \frac{t}{RA} \tag{9}$$

where t represents the thickness of the sample, R is the resistance and A is the cross-sectional area of the cell. The diameter of the cell that will be used in this test is around 9 mm which results in a cross sectional area of 63.62 mm^2.

3.6. High Temperature Test.

The high temperature test was performed in a tube furnace under vacuum pressure. The heating was done up to 200 ^oC and at completely anhydrous conditions. After heating, EIS test was applied to determine the conductivity. Comparison with previous data at room temperature and studying the thermal stability of the membranes were also assessed based on this test.

3.7. Polarization Curves

Considering an H_2/O_2 fuel cell for our model. The polarization curves may be theoretically generated by studying the relation between cell potential (V) and the current density (i). This can be done following Equations 10 and Equation 11 [71].

$$V = V_{rev} - V_{irrev} \tag{10}$$

$$V = E_r - \frac{RT}{n\alpha F}\ln\left(\frac{i}{i_o}\right) - \frac{RT}{nF}\ln\left(1 - \frac{i}{i_L}\right) - i(R_{elc} + R_{ionic}) \tag{11}$$

where E_r is the reversible potential at the standard state (1.229 V).

R is the gas constant (8,314 J/mol K).

F is Faraday Constant (96485 C/mol).

α is the charge transfer coefficient.

n is the number of mols of transferred electrons per mols of fuel (2).

i_o is the exchange current density (A/cm2).

i_L is the limiting current density (A/cm2).

T is the operating temperature.

R_{ionic} is the membrane resistance obtained from Nyquist plots or via rearranging Equation 9.

R_{elc} is the electric resistance of the cell. It can be found by utilizing Equation 12.

$$R_{elc} = \frac{l}{\sigma_e A} \tag{12}$$

where l is the length of the conductance, A is the cross sectional Area of the cell (62.63 mm^2) and σ_e is the electrical conductivity. For simplification, the length of the conductance will be assumed equal to the membrane thickness.

In addition, According to Gamalath and Peiri [72], $i_o = 1.5\ A/cm^2$, $\alpha = 0.5$ and $i_L = 10^{-6} A/cm^2$. Therefore, using experimental conductivity data for selected membranes, one may now use equation 1 to generate a relationship between current density and cell potential; hence generate polarization curves for the different fuel cell membranes.

Chapter 4. Results and Discussion

This chapter presents the results of the theoretical modelling performed on the developed PANI based membranes and evaluates their performance. It shows how the factorial design model was integrated in this work to display the effect of different factors and their interactions on proton conductivity. In addition, the chapter also explains how this model can predict the optimum conditions for all the factors for a targeted conductivity value. Finally, the performance of the developed fuel cells will be determined by analyzing the different polarization curves and compare them other PEMFCs and DEMFCs.

4.1. EIS and Theoretical Modelling

This section is going to discuss the EIS results for the synthesized membranes and how these results were integrated into a theoretical model using Minitab 19 factorial design. As illustrated earlier two factorial design models were developed. The idea of the 1st factorial design is to study the relationship between PANI concentration (A) and IL type (E). This model will show the effect of each of those two factors on the membrane conductivity; which would conclude the appropriate IL type to be used in the 2nd factorial design model.

In the 2nd factorial design, the concentration of PANI (A), IL (B) and ZrP (C) along with temperature (D) are going to be varied in order to study their effect on the membrane conductivity. Both main effect and interaction effect of these factors are to be discussed. In both models, each experiment was repeated 3 times and their average conductivity was recorded. The full factorial design data can be found in Appendix A. In addition, significant information about membrane thickness and resistance can be found in Appendix B.

4.1.1. EIS and 1st factorial design. To determine the appropriate IL type, four different membranes were synthesized using the method mentioned earlier in the methodology section. The membranes were mainly PANI/IL composite membranes supported on PTFE. The concentration of PANI was varied from 0.61 wt% to 1.22 wt% and the IL was also varied in between two types: 1-Hexyl-3-Methylimidazolium Tricyanomethanide (HMT) and Diethylmethylammonium Methanesulfonate (DEMM). The experiments' set up is illustrated in Table 9.

Table 9: Experiments conducted for the 1st FD model.

Standard Order	PANI (wt%) (A)	IL type (E)	Avg. Conductivity (S/cm)
1	0.61	1-Hexyl-3-Methylimidazolium Tricyanomethanide	0.00917
2	1.22	1-Hexyl-3-Methylimidazolium Tricyanomethanide	0.00853
3	0.61	Diethylmethylammonium Methanesulfonate	0.00357
4	1.22	Diethylmethylammonium Methanesulfonate	0.0028

Following the preparation, the synthesized membranes' conductivities were measured using the EIS test. Conductivity results showed a semi-circle response on the EIS Nyquist plot indicating that diffusional transport of ions is the measure driving force for proton transport in the cell. The conductivity can be calculated using Equation 9 after determining the resistance value from the Nyquist plot.

The real resistance/impedance (Z) value of the cell is the response intercept with the horizontal axis. For instance, for the 0.61 wt% PANI/HMT IL membrane, the resistance value was found to be 5.84Ω as shown in Figure 17. Given that the measured membrane thickness was 0.34 mm, the calculated ionic conductivity was found to be 0.00917 S/cm. When varying the PANI concentration for the same IL, the measured conductivity was found to be 0.00853 S/cm.

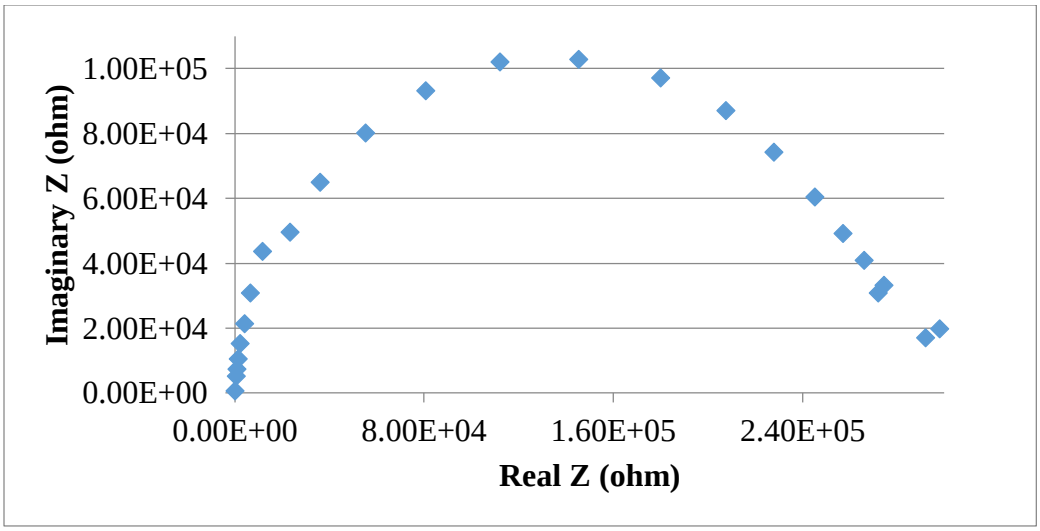

Figure 17: Experimental Nyquist plot for 0.61 wt% PANI/ HMT IL synthesized membrane.

Same Approach was used for the membranes synthesized with the DEMM IL type. As illustrated in Figure 18, the real resistance value for a 0.61 wt% PANI sample was found to be 17.16 Ω. The measured membrane thickness for this membrane was found to be 0.39 mm; resulting in a 0.00357 S/cm. When the PANI concentration was increased to 1.22 wt%, the conductivity was reported as 0.0028 S/cm.

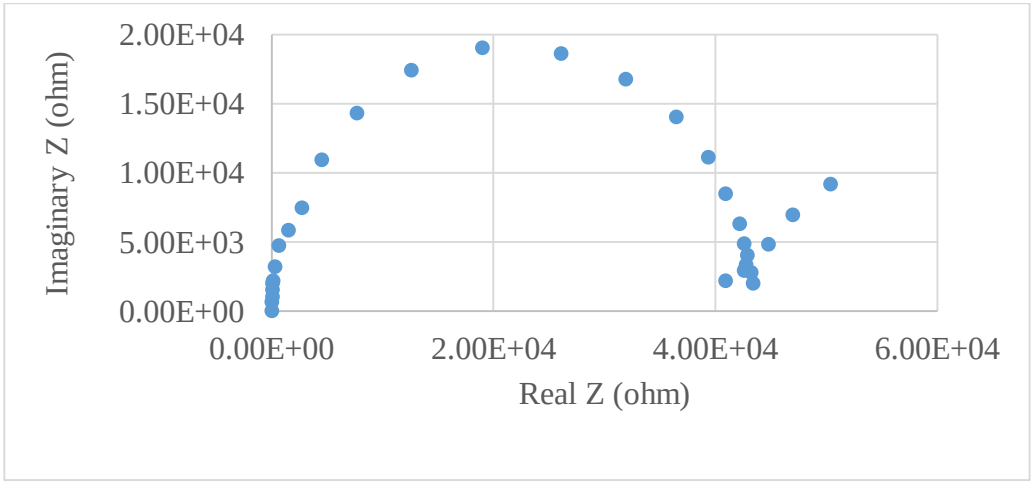

Figure 18: Experimental Nyquist plot for 0.61 wt% PANI/DEMM IL synthesized membrane.

To be able to further analyze these results, the 1st factorial design model was established. The ultimate objective of this model is to determine which IL is mostly suitable for the 2nd factorial design and also to study the effect of each factor on the membrane conductivity.

Initially, the generated model was not successful. The P-Value of the A effect and the A/E effect were 0.054 and 0.835 respectively as shown in Table 10. The Pareto chart in Figure 19 also confirms the same conclusion as it shows that A and A/E effects are below the standardized effect value of the model; meaning that they do not affect the model; on the contrary, they ruin the model.

Table 10: Coded coefficients table for the 1st FD model.

Term	**Effect**	**Coef**	**SE Coef**	**T-Value**	**P-Value**	**VIF**
Constant		0.006017	0.000155	38.87	0.000	
PANI wt%	-0.000700	-0.000350	0.000155	-2.26	0.054	1.00
IL type	0.005667	0.002833	0.000155	18.30	0.000	1.00
PANI wt%*IL type	0.000067	0.000033	0.000155	0.22	0.835	1.00

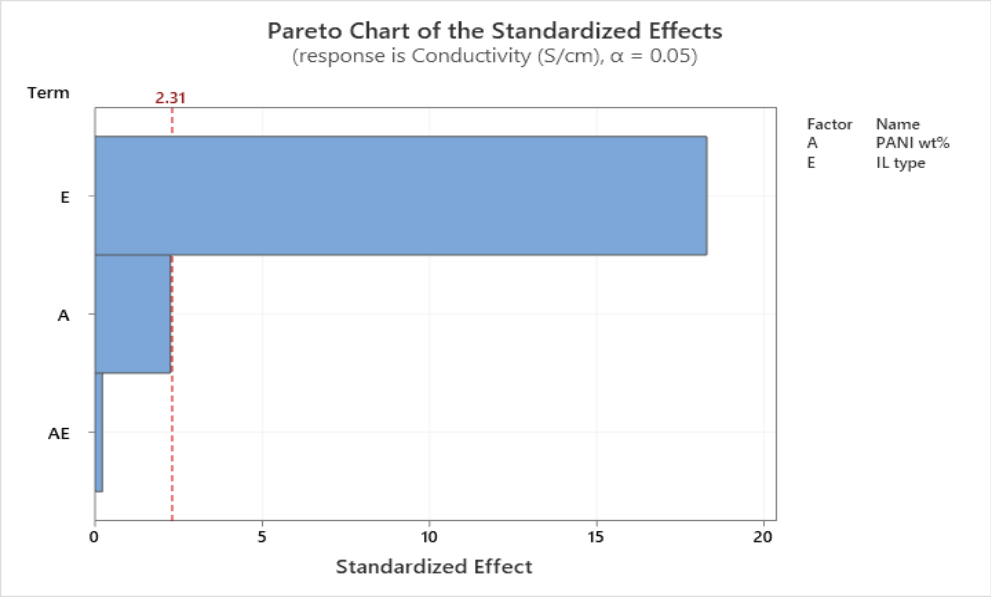

Figure 19: Pareto chart for the 1st FD model.

A successful FD model should have a P-Value of less than the significance level value (α) for all the effects. In this model, α was set to 0.05. As a result, the developed model was revised by eliminating the interaction effect between PANI concentration and IL type (the least effect) from the model. This resulted in improving the initial model by reducing the P-Value to 0.04 as shown in Table 11. The standard error (SE) coefficient (Coef) is also reasonably small. Likewise, looking at the Pareto chart in Figure 20, all the factors are now exceeding the standardized effect value. Hence, the interaction effect between PANI concentration and IL type is not desirable in this model.

Table 11: Revisited coded coefficients table for the 1st FD model.

Term	**Effect**	**Coef**	**SE Coef**	**T-Value**	**P-Value**	**VIF**
Constant		0.006017	0.000146	41.11	0.000	
PANI wt%	-0.000700	-0.000350	0.000146	-2.39	0.040	1.00
IL type	0.005667	0.002833	0.000146	19.36	0.000	1.00

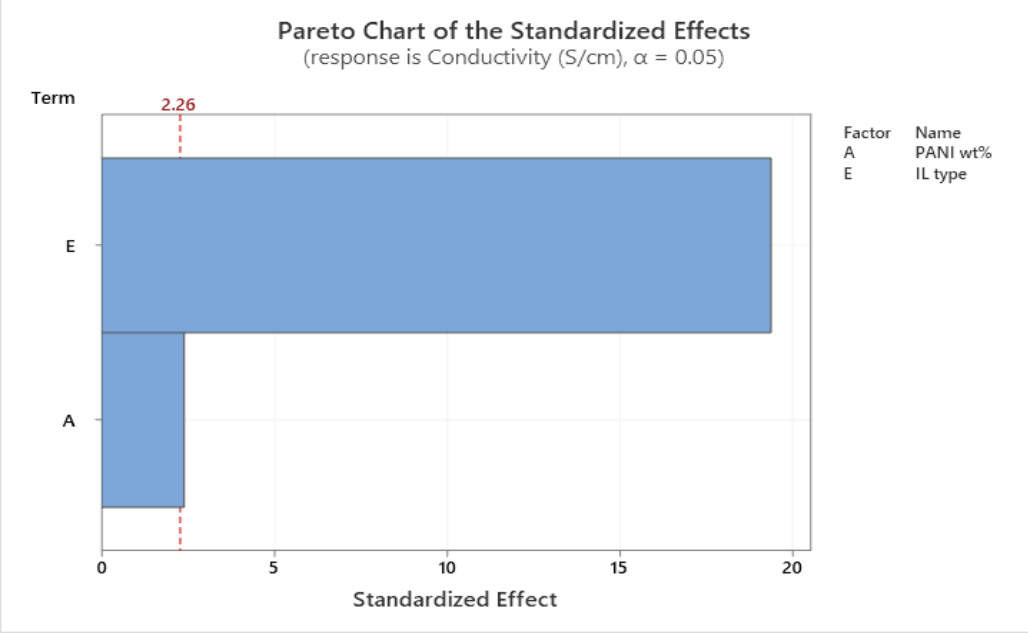

Figure 20: Revisited Pareto chart for the 1st FD model.

The new model was further proved to be valid after analyzing the model statistically. The linearity of the model was verified by looking at the R-squared value that was approximately 97.7% and an adjusted R-squared value of 97.2% as per Table 12. In addition, looking at the residual plots generated from the model in Figure 21, the normal probability plot confirms that the data are normally distributed and they fit a linear model. This can also be seen from the histogram.

Table 12: R^2 values for the 1st FD model.

S	**R^2**	**R^2(adj)**	**R^2(pred)**
0.0005070	97.69%	97.18%	95.89%

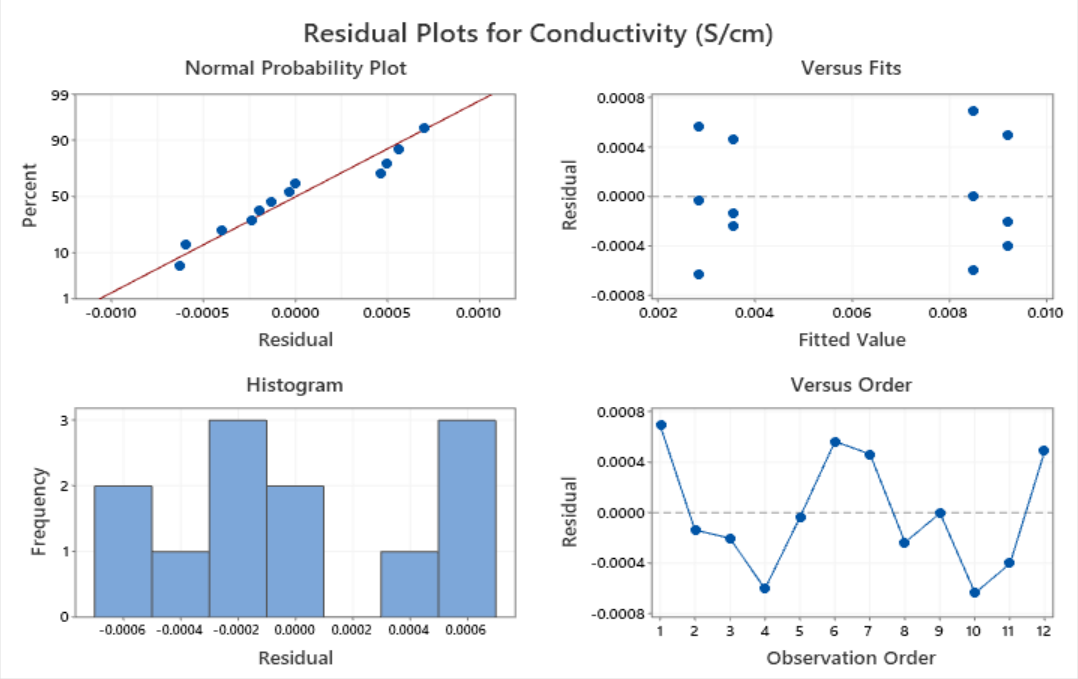

Figure 21: Residual plots for the 1st FD model.

The fitted value and the observation order plots also indicate that the data are randomly distributed, have a constant variance and the residuals are independent from each other since the data points are evenly distributed along the 0- Residual line. Therefore, the

model was considered and it was also found to adapt to the following linear regression equation (Equation 13):

$$\sigma = 0.007067 - 0.001148x_A + 0.002833X_E \quad (13)$$

where x_A and x_E are coded variables and can be determined from Table 7 as explained earlier.

4.1.1.1. ***PANI concentration effect for the 1st model.*** As discovered earlier, the concentration of PANI effect on the model is not as significant as the IL type effect. Nevertheless, it is still considered as a key factor for both this model and the 2nd FD model. Considering the conductivity results for a HMT IL type, it was shown that conductivity decreased from 0.00917 to 0.00853 S/cm when the PANI concentration (A) was increased from 0.61 to 1.22 wt%. Same behavior was noticed when increasing A for the DEMM IL type.

4.1.1.2. ***IL type effect for the 1st model***. Considering the same PANI concentration, changing the IL type was noticed to have a noticeable stronger impact on the conductivity response. Looking at a 0.61 wt% PANI concentration, it was noticed that conductivity results were 0.00357 and 0.00917 S/cm for DEMM and HMT IL types respectively. A difference of approximately 257%. This can be explained by the fact that the HMT IL type has more free H^+ ions that promote proton transport. In addition, HMT IL is actually an imidazolium type; which has an N atom in the imidazolium ring in the cation form (positive charge) as shown in Figure 22.

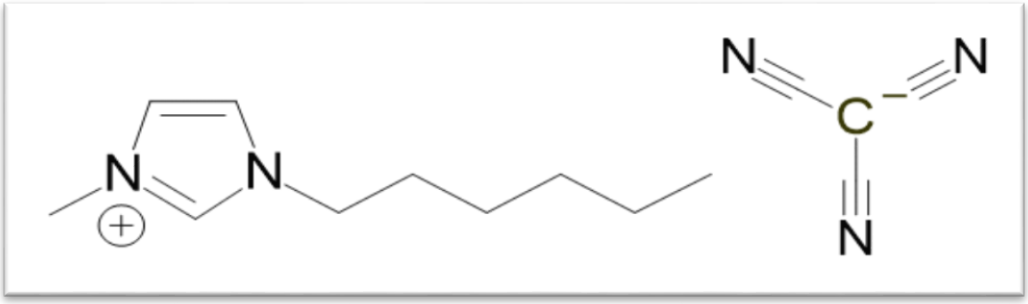

Figure 22: HMT IL chemical structure.

Furthermore, as far as ILs are concerned, proton conductivity is usually inversely proportional to viscosity and molar volume [73]. Investigating the viscosity of both IL types, it was found that viscosity of the HMT type is 39.2 cP, compared to 111 cP for the DEMM type at 25 ^{o}C [74]. Therefore, it is fair to conclude that the HMT type would have a much higher conductivity since it has a significantly lower viscosity.

Ultimately, what can be concluded from this FD study is that the HMT IL type is a much better IL to use for the 2nd FD model. The study also showed that the changing E has a stronger effect on the model than changing A. This can also be visually judged by looking at Figure 23, which shows that in the case of IL, the line is steeper. Furthermore, the study confirmed that the model is linear and the results were normally and randomly distributed as per the regression plots that were discussed earlier.

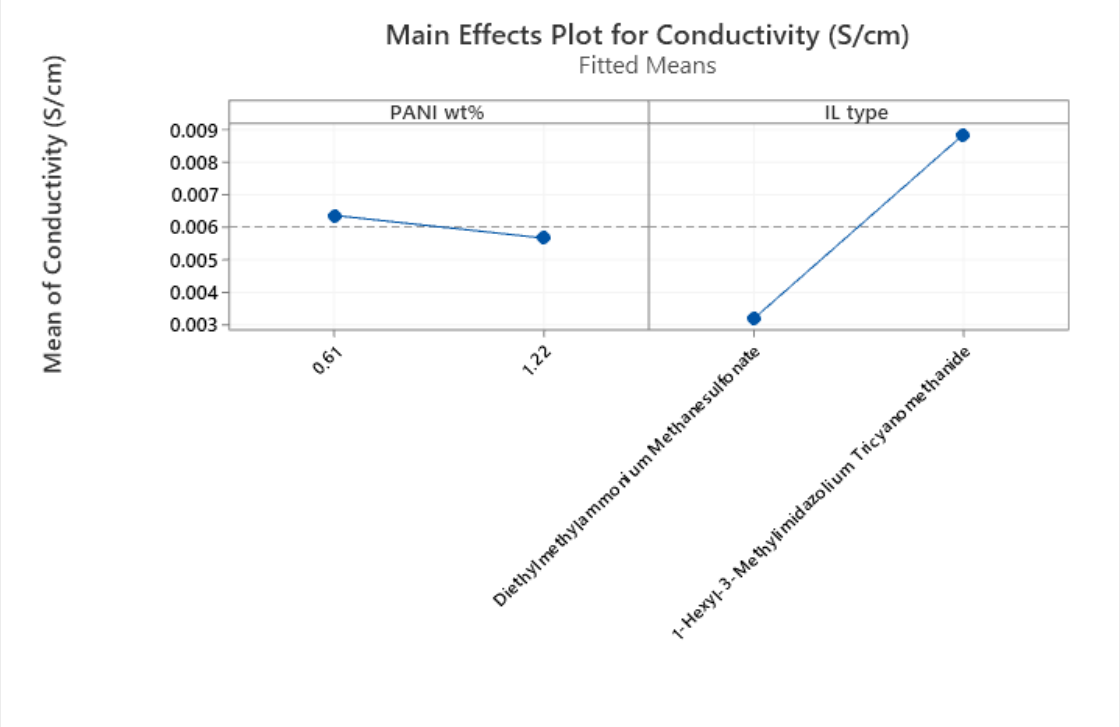

Figure 23: Main effect results for the 1st FD model.

4.1.1.3. ***Factors' contribution for the 1st model.*** Similar interpretation to the main effect and Pareto charts can be concluded from Table 13. The table presents the percentage

contribution of each factor on the response. The percentage contribution is mainly the percentage of the sum of the squares (SS) with respect to the total SS. In this model, the IL type (E) contributes by more than 96 % to the conductivity of the membrane compared to less than 1.5% provided by PANI concentration (A). A pure error of 2.3% was also detected in the model. This error was mainly due to the small sample size. In addition, it might be due to the fact that interaction effects were omitted and only linear effects were considered in this model.

Table 13: Percentage contribution and sum of the squares analysis for the 1st model.

Source	Seq SS	Contribution	Adj SS	Adj MS
Model	0.000098	97.69%	0.000098	0.000049
Linear	0.000098	97.69%	0.000098	0.000049
PANI wt%	0.000001	1.47%	0.000001	0.000001
IL type	0.000096	96.22%	0.000096	0.000096
Error	0.000002	2.31%	0.000002	0.000000
Lack-of-Fit	0.000000	0.01%	0.000000	0.000000
Pure Error	0.000002	2.30%	0.000002	0.000000
Total	0.000100	100.00%		

4.1.2. EIS and 2nd factorial design. After the appropriate IL type was determined, it was very essential to study the effect of the different factors mentioned earlier on the ionic conductivity. Since 4 factors to be studied, 16 (2^4) experiments will be required for a 2-level FD model. The experiments were mainly pure PANI, PANI/IL, PANI/ZrP and PANI/IL/ZrP membranes synthesized at different concentrations of A (0.61 and 1.22 wt%), different concentrations of B (0 and 2.5 wt%), different concentration of C (0 and 0.61 wt%) and a variation of D from 25 to 180 ^oC.

In this factorial design, most of the experimental data at 180 ^oC were not available. Hence, these data were interpolated based on the following assumptions:

1) Fully anhydrous conditions
2) The conductivity of pure PANI at high temperatures is 5 times lower than it is at room temperature [75].

3) The addition of IL will have the same effect at low and high temperatures.
4) The effect of increasing PANI wt% will be the same at high temperature
5) ±5% error at high temperature.

Applying the above listed assumptions, the missing experimental data was calculated and recorded as shown in Table 14. The experiments were then randomly ran and the conductivity was determined using the EIS approach. The calculations of the predicted values are found in Appendix B.

Table 14: Experiments conducted for the 2nd FD model.

Standard Order	**PANI wt% (A)**	**IL wt% (B)**	**ZrP wt% (C)**	**Temperature (°C) (D)**	**Avg. Conductivity (S/cm)**
1	0.61	0	0	25	0.00090
2	1.22	0	0	25	0.00080
3	0.61	2.5	0	25	0.0092
4	1.22	2.5	0	25	0.0085
5	0.61	0	0.61	25	0.00076
6	1.22	0	0.61	25	0.00057
7	0.61	2.5	0.61	25	0.020
8	1.22	2.5	0.61	25	0.0085
9	0.61	0	0	180	0.00018
10	1.22	0	0	180	0.00016
11	0.61	2.5	0	180	0.0018
12	1.22	2.5	0	180	0.0017
13	0.61	0	0.61	180	0.00015
14	1.22	0	0.61	180	0.00011
15	0.61	2.5	0.61	180	0.020
16	1.22	2.5	0.61	180	0.0084

The pure PANI membrane demonstrated a resistance of 54.1Ω as shown in Figure 24 for the 0.61 wt% sample. The membrane thickness was measured at 0.3 mm resulting in a 0.0009 S/cm ionic conductivity. Same approach was used for the 1.22 wt% sample and resulted in a proton conductivity of 0.0008 S/cm. When both membranes were interpolated at high temperatures, the proton conductivity results were 0.000887 and 0.000788 S/cm respectively.

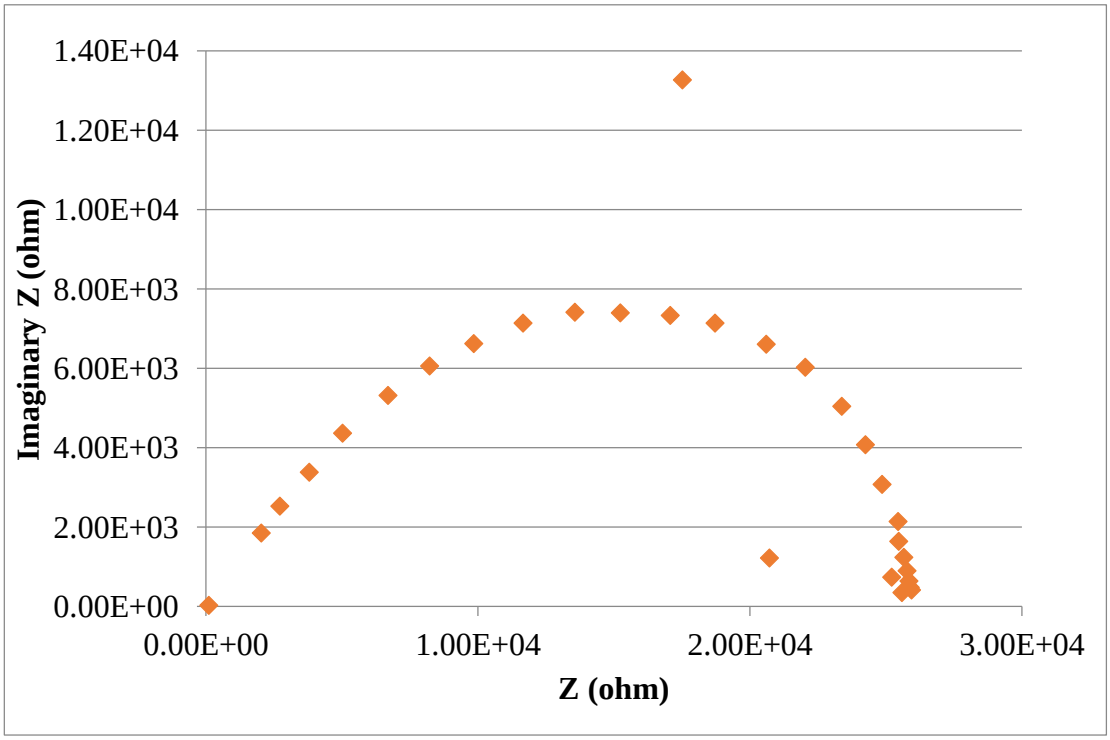

Figure 24: Experimental Nyquist plot for pure 0.61 wt% PANI synthesized membrane.

For the PANI/IL membrane samples, the results were taken from the 1st FD model using the HMT IL type; 0.00917 and 0.00853 S/cm for 0.61 and 1.22 wt% of PANI respectively, since the concentration of IL used in the 1st model was also 2.5 wt% and the temperature was also the same; maintained at 25 ^{o}C. Besides, when membranes were modelled at high temperatures, conductivity results were 0.008867 and 0.0084 S/cm in the same order.

The EIS results when 0.61wt% of ZrP was introduced to a pure PANI membrane (0.61 wt%) showed a resistance of 123.4Ω as shown in Figure 25. The measured thickness of the membrane was found to be around 0.6mm. Therefore, the calculated conductivity is 0.000757 S/cm. When the 1.22 wt% PANI was mixed with ZrP, a 0.000567 S/cm ionic conductivity was obtained using the same approach. Upgrading to high temperature operations, ionic conductivity results were found to be 0.000746 and 0.000599 S/cm respectively.

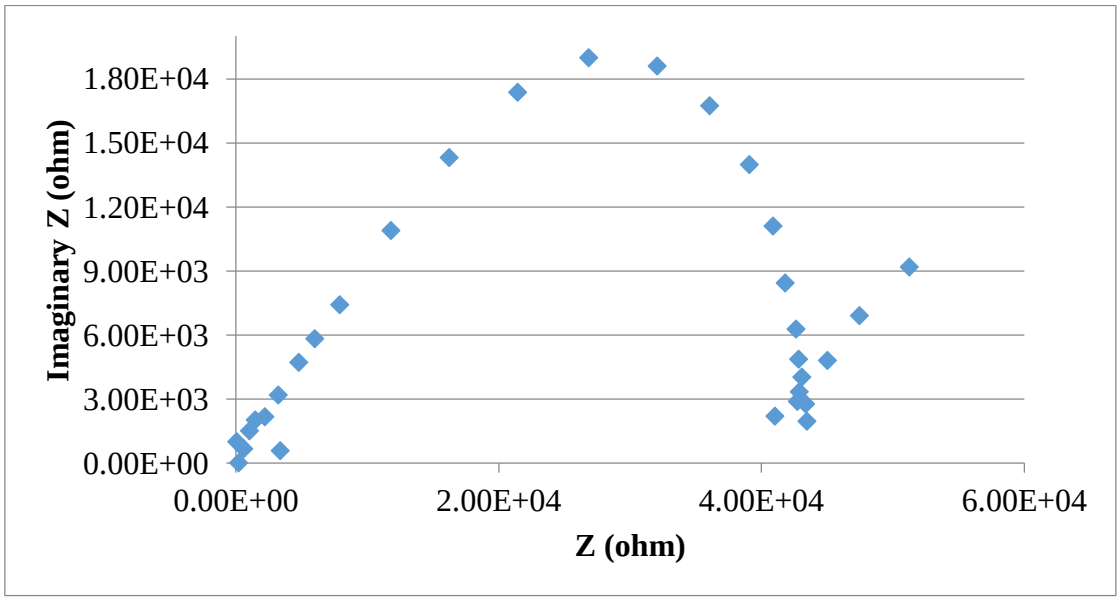

Figure 25: Experimental Nyquist plot for pure 0.61 wt% PANI, 0.61 wt% ZrP composite synthesized membrane.

Ultimately, when a composite membrane of PANI, IL and ZrP was synthesized, a remarkable resistance of 4.4Ω was obtained for a 0.6 mm membrane as viewed in Figure 26. This resulted in an ionic conductivity of 0.0203 S/cm for a 0.61 wt% PANI membrane and 0.0085 S/cm for a 1.22 wt% PANI membrane. The 1st membrane underwent high temperature test at an anhydrous conditions and the resulted ionic conductivity was 0.02 S/cm. The other membrane was modelled accordingly and resulted in a conductivity of 0.00837 S/cm.

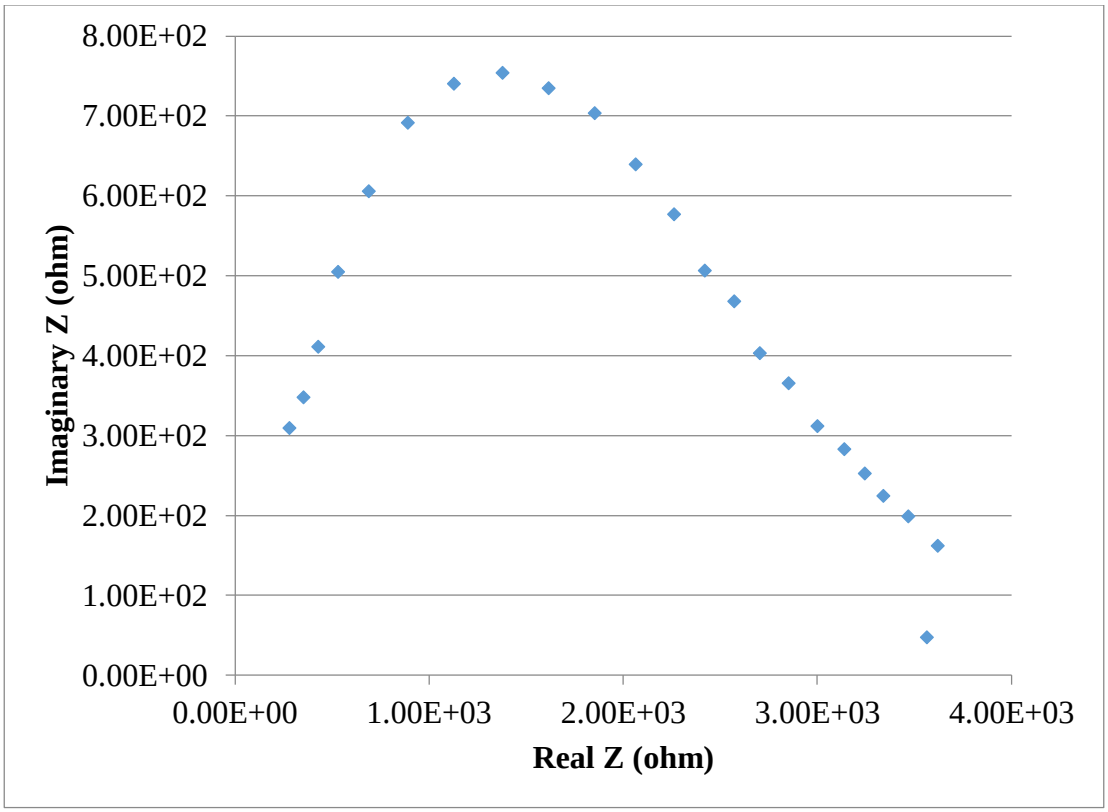

Figure 26: Experimental Nyquist plot for pure 0.61 wt% PANI, 0.61 wt% ZrP, 2.5 wt% HMT IL synthesized composite membrane.

Considering the 2nd factorial design, one may analyze the obtained results and study the effect of the different factors on the conductivity response. Similar to the 1st factorial design, the 1st model was unsuccessful and presented P-Values that are higher than the $\alpha = 0.05$ value indicating that some terms are insignificant in the model as illustrated in Table 15.

Eliminating the terms that are lower than the standardized effect value of 2.04 as shown in Figure 27, resulted in a more reliable model that has a negligible P-Values as can be seen from Table 16. The eliminated terms were mainly the PANI interaction with temperature (AD), PANI interaction with temperature and IL (ABD), PANI interaction with temperature and ZrP (ACD) and the interaction of PANI with all the factors combined (ABCD). These terms are undesirable in the model. The remaining terms can be clearly seen from Figure 28.

Table 15: Coded coefficients table for the 2nd FD model.

Term	Effect	Coef	SE Coef	T-Value	P-Value	VIF
Constant		0.005126	0.000090	56.65	0.000	
PANI wt%	-0.003078	-0.001539	0.000090	-17.01	0.000	1.00
IL wt%	0.009358	0.004679	0.000090	51.71	0.000	1.00
ZrP wt%	0.004433	0.002216	0.000090	24.49	0.000	1.00
Temperature (C)	-0.002124	-0.001062	0.000090	-11.74	0.000	1.00
PANI wt%*IL wt%	-0.002978	-0.001489	0.000090	-16.46	0.000	1.00
PANI wt%*ZrP wt%	-0.002857	-0.001429	0.000090	-15.79	0.000	1.00
PANI wt%*Temperature (C)	0.000124	0.000062	0.000090	0.68	0.499	1.00
IL wt%*ZrP wt%	0.004558	0.002279	0.000090	25.19	0.000	1.00
IL wt%*Temperature (C)	-0.001532	-0.000766	0.000090	-8.46	0.000	1.00
ZrP wt%*Temperature (C)	0.001756	0.000878	0.000090	9.70	0.000	1.00
PANI wt%*IL wt%*ZrP wt%	-0.002818	-0.001409	0.000090	-15.57	0.000	1.00
PANI wt%*IL wt%*Temperature (C)	0.000053	0.000027	0.000090	0.29	0.770	1.00
PANI wt%*ZrP wt%*Temperature (C)	-0.000022	-0.000011	0.000090	-0.12	0.902	1.00
IL wt%*ZrP wt%*Temperature (C)	0.001668	0.000834	0.000090	9.22	0.000	1.00
PANI wt%*IL wt%*ZrP wt%*Temperature (C)	-0.000053	-0.000026	0.000090	-0.29	0.772	1.00

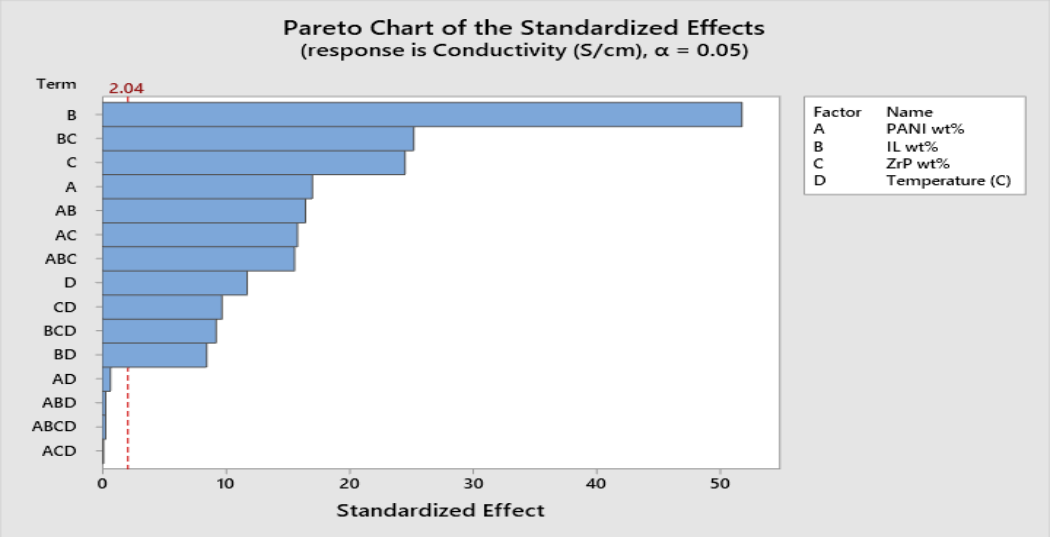

Figure 27: Pareto chart for the 2nd FD model.

Table 16: Revisited coded coefficients table for the 2nd FD model.

Term	**Effect**	**Coef**	**SE Coef**	**T-Value**	**P-Value**	**VIF**
Constant		0.005126	0.000086	59.48	0.000	
PANI wt%	-0.003078	-0.001539	0.000086	-17.86	0.000	1.00
IL wt%	0.009358	0.004679	0.000086	54.29	0.000	1.00
ZrP wt%	0.004433	0.002216	0.000086	25.72	0.000	1.00
Temperature (C)	-0.002124	-0.001062	0.000086	-12.32	0.000	1.00
PANI wt%*IL wt%	-0.002978	-0.001489	0.000086	-17.28	0.000	1.00
PANI wt%*ZrP wt%	-0.002857	-0.001429	0.000086	-16.58	0.000	1.00
IL wt%*ZrP wt%	0.004558	0.002279	0.000086	26.44	0.000	1.00
IL wt%*Temperature (C)	-0.001532	-0.000766	0.000086	-8.89	0.000	1.00
ZrP wt%*Temperature (C)	0.001756	0.000878	0.000086	10.19	0.000	1.00
PANI wt%*IL wt%*ZrP wt%	-0.002818	-0.001409	0.000086	-16.35	0.000	1.00
IL wt%*ZrP wt%*Temperature (C)	0.001668	0.000834	0.000086	9.68	0.000	1.00

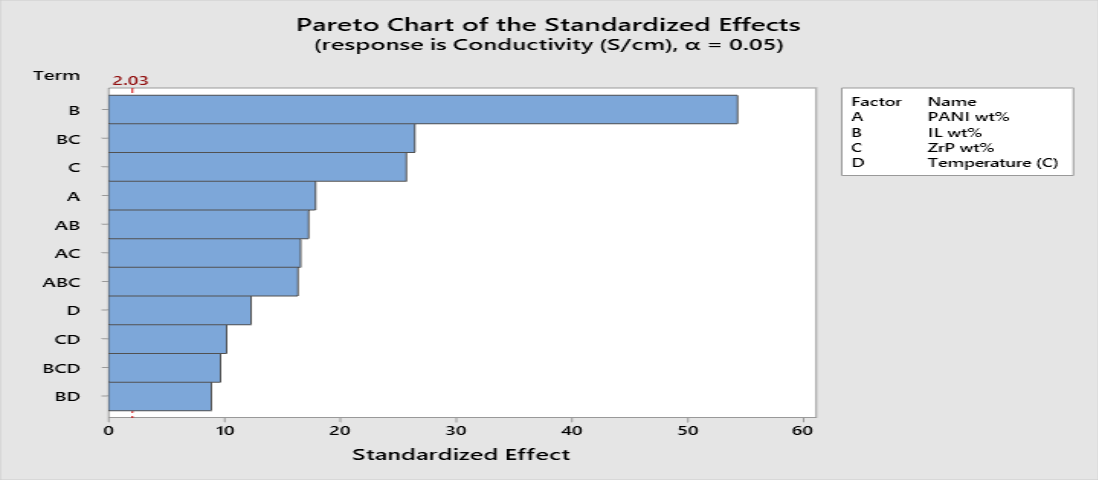

Figure 28: Revisited Pareto Chart for the 2nd FD model.

The new model has an S-shaped normality plot. The S-shaped distribution indicates long tails in the model which may be a result of not enough data points. This can be confirmed from the fitted value plot that shows a non-constant variance in the data as well as the variations in T-values. Nevertheless, the model has a 99% R-squared regression and the histogram tend to follow a normal distribution which verifies the applicability of the model as can be seen from Table 17 and Figure 29.

In addition, the model appeared to follow the linear equation presented below

$$\sigma = 0.001050 - 0.000099x_A + 0.003805x_B - 0.00020x_c - 0.000004x_D - 0.000210x_Ax_B - 0.00021x_Ax_C + 0.014172x_Bx_C - 0.000017x_Bx_D + 0.000002x_Cx_D - 0.012117x_Ax_Bx_C + 0.000028x_Bx_Cx_D \quad (14)$$

where x_A x_B x_C and x_D are coded variables and can be determined from Table 8 as illustrated previously.

Table 17: R^2 values for the 2nd FD model

S	**R^2**	**R^2(adj)**	**R^2(pred)**
0.0005971	99.39%	99.21%	98.92%

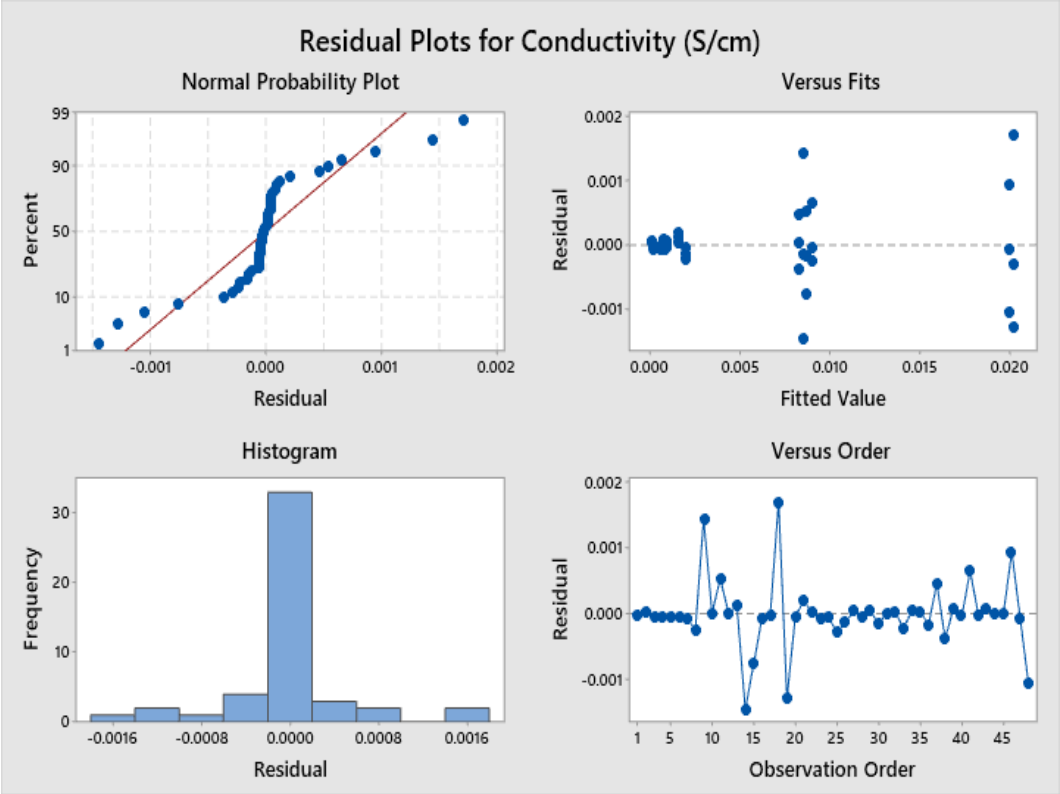

Figure 29: Residual plots for the 2nd FD model.

4.1.2.1. ***PANI concentration effect for the 2nd model.*** The impact of increasing the PANI concentration resulted in a decrease in conductivity at both room and high temperatures. At room temperature the decrease can be explained by the fact that more PANI molecules block the capability of protons to pass freely through the membrane. Unlike the 1st FD model, the concentration of PANI (A) is considered very significant in the design of this model. In fact, a decrease of 0.0035 S/cm in the mean conductivity can be estimated from Figure 30.

4.1.2.2. ***IL concentration effect for the 2nd model.*** Similar to the 1st FD design model, the effect of the addition of IL is considered the most important variable in this model. The HMT IL demonstrated a remarkable increase in the mean conductivity value that reached 0.0095 S/cm as can be seen from the main effect plot. As mentioned earlier, this is due to the HMT structure that has a cation N in the imidizolium ring that promotes proton transport.

4.1.2.3. *ZrP concentration effect for the 2nd model.* The addition of ZrP is actually found the 3rd important factor in this model. This can be explained by the fact that ZrP plays a serious role in the mechanical and thermal stability of the membrane as well as weak acidic groups that allow protons transport freely.

When utilized with PANI alone, the conductivity was noticed to shrink. However, when used with both PANI and IL, the membrane conductivity was found to increase dramatically up to 0.0203 S/cm at room temperature. Therefore, the mean conductivity response showed an increase of 0.006 S/cm in this model.

4.1.2.4. *Temperature effect for the 2nd model.* The effect of increasing temperature to 180 ^{o}C resulted in a decrease in conductivity in general. This can be explained by the fact that at high temperature, membrane would dehydrate. In addition, the IL would start to evaporate also at high temperature resulting in a decrease in conductivity. Looking at the main effect plot, the temperature would cause a decrease of 0.0025 S/cm in the model.

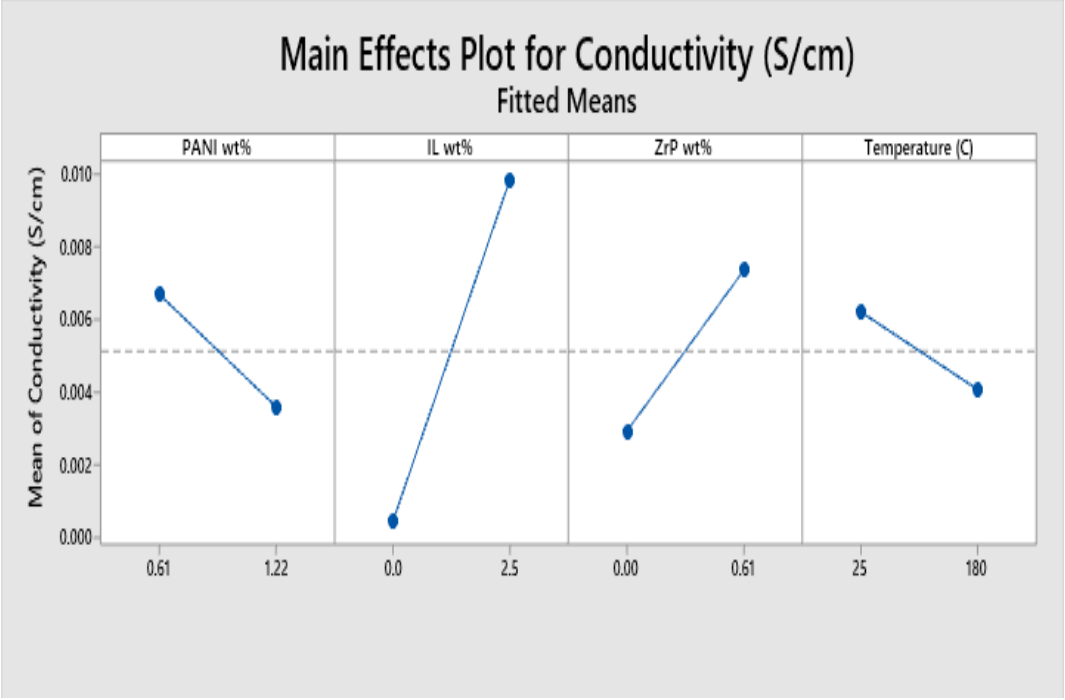

Figure 30: Main effect results for the 2nd FD model.

4.2.2.5. *Interaction effects for the 2nd model.* The interaction between the different 4 factors are very important for this model. Mainly, the interaction between IL and ZrP concentrations (BC), PANI and IL concentrations (AB) interaction, PANI and ZrP concentrations (AC) effect and the interaction between PANI IL and ZrP concentrations (ABC) all together. In addition, the interaction of temperature with ZrP (CD), IL (BD) and with IL and ZrP (BCD) all together are also fairly important in this model.

Looking at BC interaction, it is noticed that conductivity increases dramatically when IL and ZrP are introduced together. A 0.015 S/cm increase in the mean conductivity response was simulated as shown in Figure 31. This is due to the fact that both IL and ZrP are hydrophilic and their combination enhances proton transfer.

Unlike BC interaction, when ZrP was mixed with PANI (AC), a negative response on the conductivity was observed. Conductivity decreased by a factor of 0.006 S/cm on the mean conductivity response. This is reasonable since both factors independently tend to decrease the conductivity as illustrated earlier.

When it comes to AB effect, the mean conductivity was found to actually decrease from 0.0125 to 0.007 S/cm. Although the effect of B alone causes a dramatic increase in conductivity, still when interacted with A, it seems that the overall result would decrease the conductivity according to this model.

As far as temperature is concerned, a remarkable increase was observed when interacted with IL (BD) and also a less significant increase was also noted when interacted with ZrP (CD).

For the three way interactions; mainly ABC and BCD, their plots were not available. However, it can be fairly assumed that ABC would decrease the mean conductivity response unlike BCD. Both AB and BC interactions decreased the conductivity independently and hence their combination would also decrease the response. Similarly, Both BD and CD increased the mean conductivity value and therefore, their combination would also result in a higher mean response.

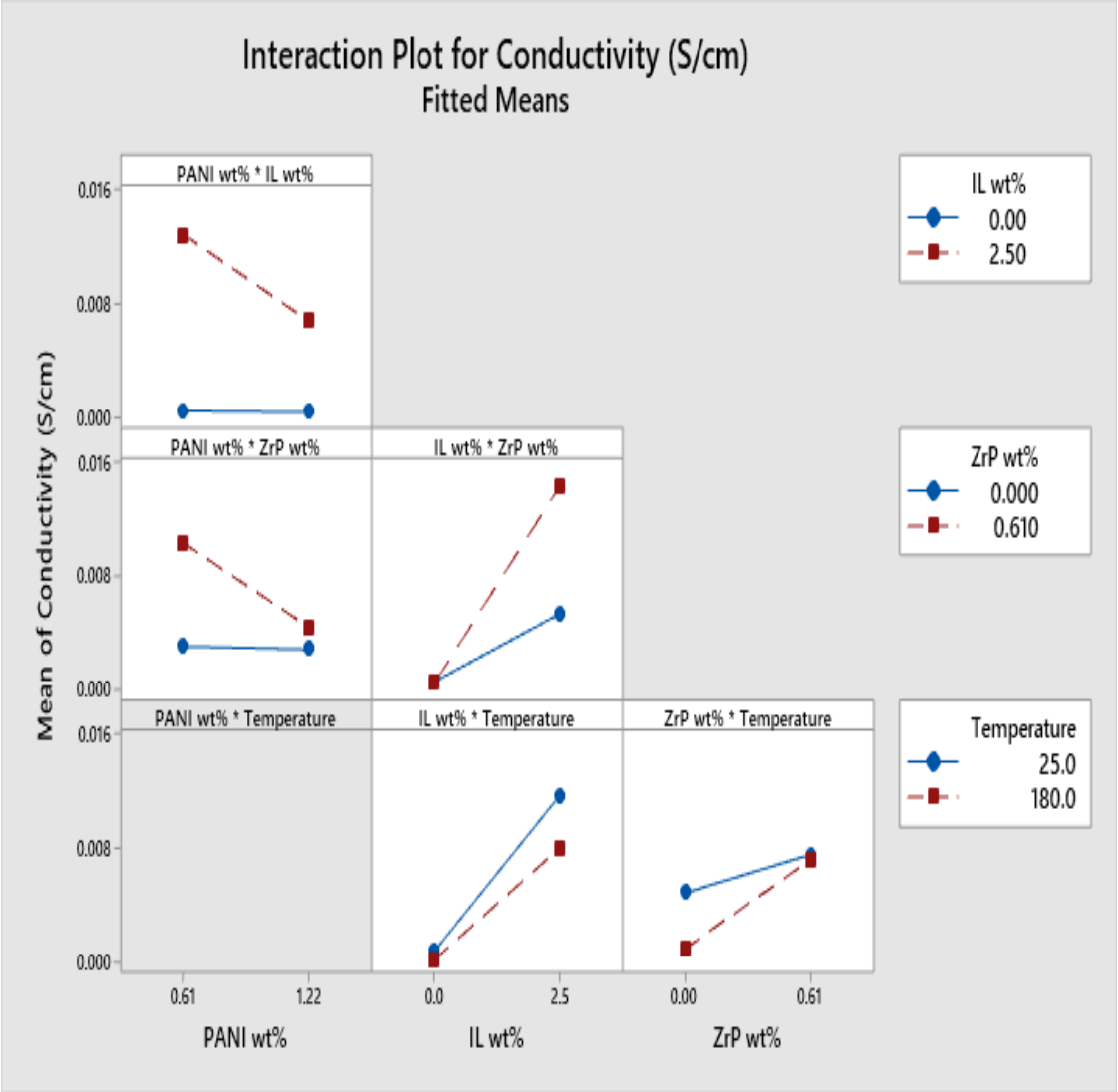

Figure 31: Interaction effect for the 2nd FD model.

4.2.2.6. ***Factors' contribution for the 2nd model***. The linear effects contributed by nearly 69% to the conductivity response, where the 2-way and the 3-way interactions contributed by 24.5% and 6% respectively. In the linear effects, as discussed earlier, the dominating factor was the IL concentration (B); which had almost 50% contribution to the membrane's conductivity. Where for the interaction effects, the main interaction that affected the response was between IL and ZrP concentrations (BC). The BC interaction contributed by almost 12% to the model response. The contribution percentage of all the factors can be found in Table 18.

Table 18: Percentage contribution and sum of the squares analysis for the 2nd model.

Source	Seq SS	Contribution	Adj SS	Adj MS
Model	0.002102	99.39%	0.002102	0.000191
Linear	0.001454	68.77%	0.001454	0.000364
PANI wt%	0.000114	5.38%	0.000114	0.000114
IL wt%	0.001051	49.69%	0.001051	0.001051
ZrP wt%	0.000236	11.15%	0.000236	0.000236
Temperature (C)	0.000054	2.56%	0.000054	0.000054
2-Way Interactions	0.000519	24.54%	0.000519	0.000104
PANI wt%*IL wt%	0.000106	5.03%	0.000106	0.000106
PANI wt%*ZrP wt%	0.000098	4.63%	0.000098	0.000098
IL wt%*ZrP wt%	0.000249	11.79%	0.000249	0.000249
IL wt%*Temperature (C)	0.000028	1.33%	0.000028	0.000028
ZrP wt%*Temperature (C)	0.000037	1.75%	0.000037	0.000037
3-Way Interactions	0.000129	6.08%	0.000129	0.000064
PANI wt%*IL wt%*ZrP wt%	0.000095	4.51%	0.000095	0.000095
IL wt%*ZrP wt%*Temperature (C)	0.000033	1.58%	0.000033	0.000033
Error	0.000013	0.61%	0.000013	0.000000
Lack-of-Fit	0.000000	0.01%	0.000000	0.000000
Pure Error	0.000013	0.59%	0.000013	0.000000
Total	0.002115	100.00%		

4.2. Cell Performance

To further analyze the performance of the synthesized membranes, polarization curves for selected membranes were generated. Polarization curves show the performance of the fuel cell as opposed to what is predicted by thermodynamics. The curves were theoretically developed using Equation 11. The generated polarization curves were further compared with literature data for different PEMFCs and DMFCs to ensure that the performance of the synthesized membranes aligns with the performance of known

membranes. The selected membrane for the analysis covered all combinations; from pure PANI, PANI/IL and PANI/IL/ZrP membranes at both room temperature and 180 ºC as illustrated in Table 19.

Table 19: Data for selected membranes.

PANI (wt%)	**IL (wt%)**	**ZrP (wt%)**	**Temperature (ºC)**	**σ_i (S/cm)**	**R_{ionic}* (Ω)**	**σ_e (S/cm)**	**R_{elc} (Ω)***
0.61	0	0	25	0.00090	54.1	3.5 [76]	0.013
0.61	0	0	180	0.00018	436.60	2×10^{-5} [76]	2357.75
0.61	2.5	0	25	0.0092	5.84	120 [60]	0.00045
0.61	2.5	0	180	0.0018	42.85	10 [60]	0.0053
0.61	0	0.61	25	0.00076	123.4	1.8×10^{-4} [77]	523.94
0.61	0	0.61	180	0.00015	520.47	4×10^{-3} [77]	23.58
0.61	2.5	0.61	25	0.020	4.40	77.7 *	0.0012
0.61	2.5	0.61	180	0.020	4.90	32.634*	0.0030

Note: Calculations of predicted values of σ_e are available in Appendix B. High temperature values of R_{ionic} can be found via rearranging Equation 9. Values of R_{elc} were found via rearranging Equation 12.

The results showed that Pure PANI membranes would have a decent stability and can provide a current density up to 0.008 A/cm^2 at a cell potential as low as 0.28 V. This result by far overthrows that from the literature. According to Gharibi et al. [78], at the same potential, only 0.000125 A/cm^2 current density can be generated. This indicates that PANI prepared in this work which was doped in HCL is by far more conductive, stable and provides more current that that from literature as can be seen from Figure 32.

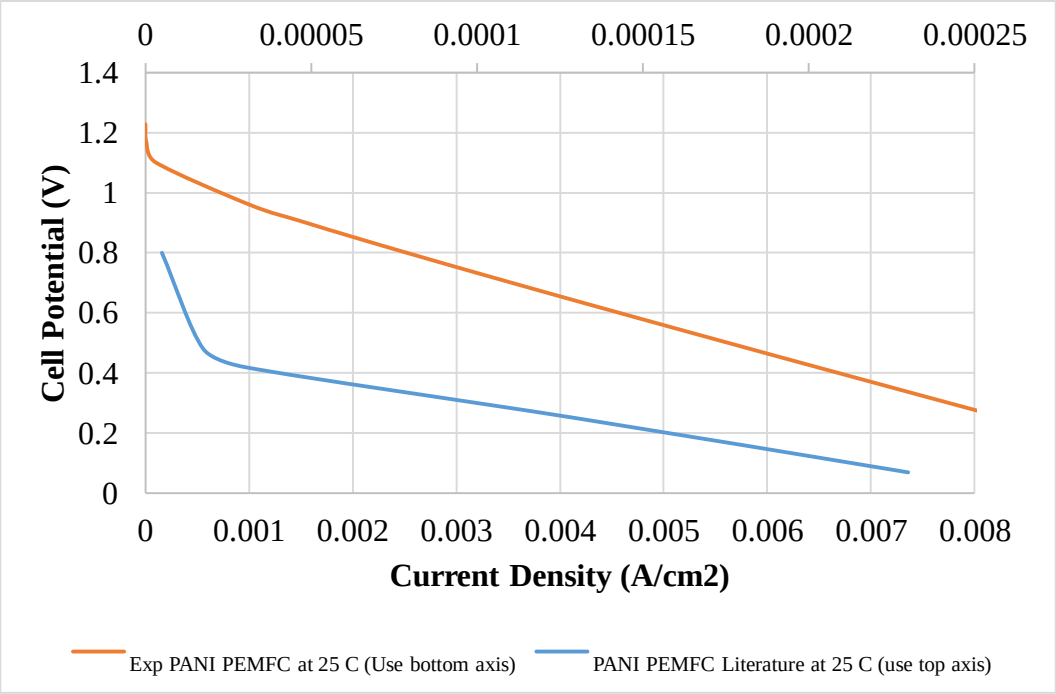

Figure 32: Polarization curves for pure PANI.

When IL was introduced, the cell performance was noticed to improve specially at room temperature. At a cell potential of 0.70 V, the synthesized PANI/IL membrane showed that it can provide a current densities up to 0.0045 and 0.03 A/cm^2 at 180 ^{o}C and room temperature respectively as presented in Figure 33. High temperature Nafion membrane when fabricated with IL gave only 0.003 A/cm^2 current density at the same potential [17]. Therefore, it is fair to conclude that IL more impact when mixed with PANI; resulting in a more stable membrane. Although the PANI/IL membrane is not stable at high temperature, it can still be improved by the addition of ZrP.

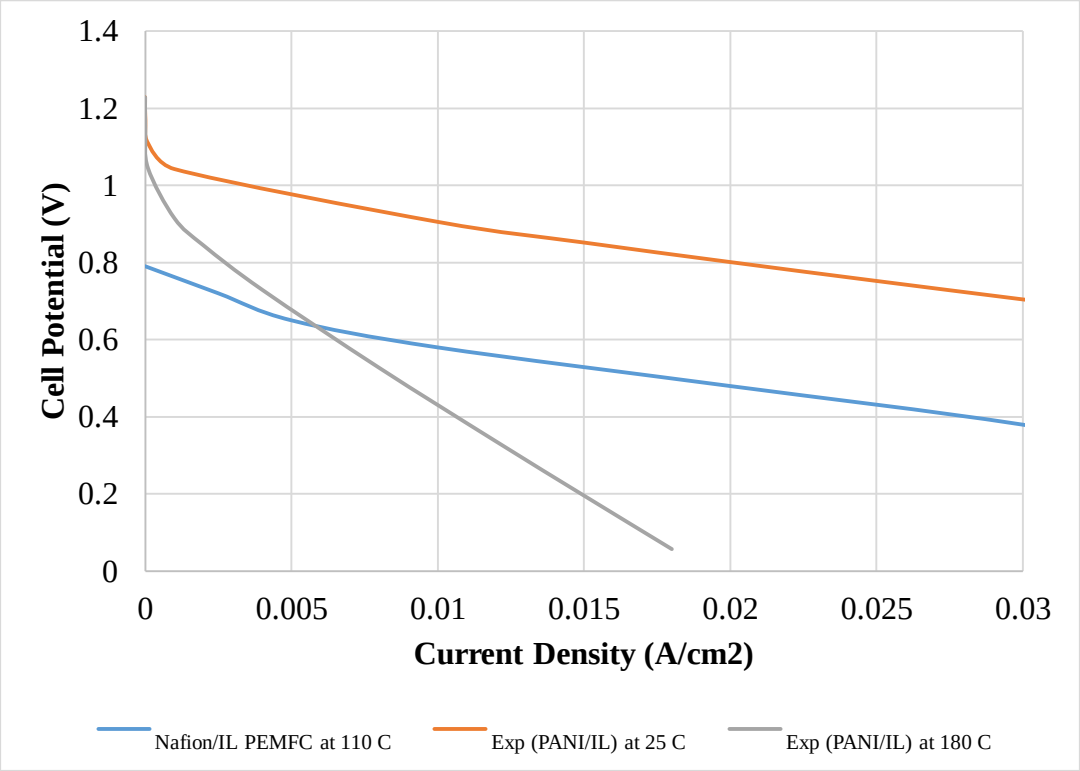

Figure 33: Polarization curves for the PANI/IL membranes compared to a Nafion/IL membrane.

When ZrP was introduced to PANI and IL, the developed membrane showed a substantial increase in current density and stability. At room temperature, with a cell potential of 0.54 V, the membrane reached a current density of 0.1 A/cm^2 as demonstrated in Figure 34. At 180 ºC, the value drops slightly to 0.055 A/cm^2 at the same potential. Compared to Espasandín et al. [79] Nafion membrane, the synthesized membrane managed to reach the same current density at a lower potential.

The performance of the cell dropped to its half at high temperature since the generated current density at the same potential was around 0.052 A/cm^2. The performance was observed to be lower than that of a PBI PEMFC, which reaches a current density higher than 0.2 A/cm^2 at the same potential of 0.54 V [80]. Nevertheless, the synthesized membrane showed a better performance than that of Nafion and Nafion/ZrP in a DMFCs. Their generated current densities only reached around 0.03 A/cm^2 at the same potential [81].

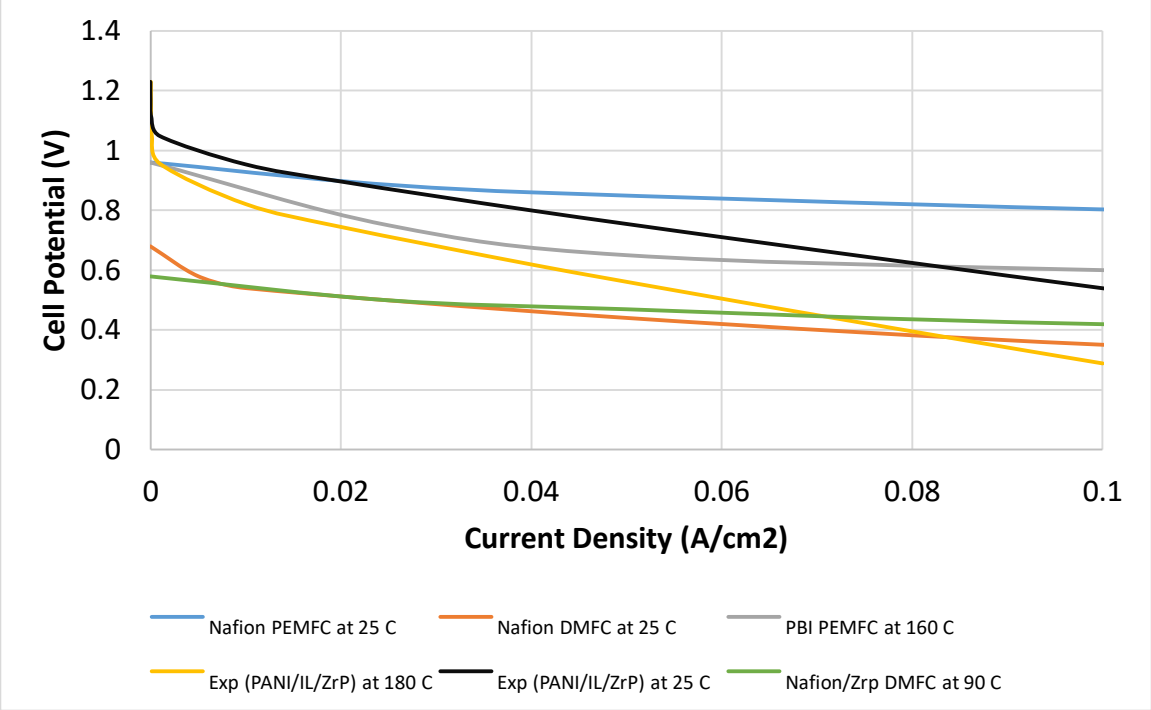

Figure 34: Polarization curves of PANI/ZrP/IL membranes compared to other widely-used membranes.

4.3 Results Summary and Further discussion

Considering the results obtained and discussed earlier in terms of conductivity and cell performance, they can be summarized in Table 20 below. Membrane conductivities obtained from this work compete fairly with results obtained from literature. More specifically, although its conductivity was found to be 21% of Nafion's at room temperature, the PANI/ZrP/IL composite membrane demonstrated a reasonable proton conductivity characteristics. Not only it was conductive, but it also demonstrated high thermal stablity at 180 ^{o}C unlike Nafion and other membranes investigated in this work.

The composite membrane' conductivity almost stayed at the same when treated at high temperatures. Where for Nafion, only at 130 ^{o}C, its conductivity dropped by more than 84%. In addition, at 180 ^{o}C, Nafion is expected to suffer and extreme drop in conductivity and cell performance in general [82]. This confirms the adequacy of the synthesized membrane; especially that sufficient current density is provided at both low and high temperatures.

In addition to its thermal stability and its ability to generate current, synthesizing such a membrane in an H_2/O_2 fuel cell and operating it at high temperatures would have several of other advantages. First, there will be no need for a major water management system, since most of the water will evaporate before 180 ^oC; which means lower operating cost. Furthermore, via utilizing H_2 as the fuel of the cell, the platinum catalyst will be protected from CO deposits. In addition, faster kinetics is guaranteed at high temperatures which will enhance the proton and current transfers.

Table 20: Summary of the results.

Membrane	**Conductivity (S/cm)**	**Temperature (^oC)**	**Current density at 0.6 V (A/cm^2)**	**Reference**
PANI	0.00090	25	0.0045	This work
PANI	0.00018	180	1.05×10^{-5}	This work
PANI/IL	0.0092	25	0.042	This work
PANI/IL	0.0018	180	0.060	This work
PANI/ZrP/IL	0.0203	25	0.082	This work
PANI/ZrP/IL	0.0200	180	0.042	This work
Nafion 117	0.094	25	0.6	[17]
Nafion 115	0.015	180	Extremely low	[82]
PANI	10-4	25	2.1×10^{-5}	[78]
PANI	2×10^{-5}	180	-	[76]
PBI	0.023	25	-	[83]
PBI	0.0667	160	-	[43]
SPEEK	0.048	25	-	[84]
SPEEK	0.067	120	-	[45]

Chapter 5. Conclusion and Future Work

This chapter is going to conclude the thesis by illustrating the thesis objectives and how they were met. The chapter will also address future room for improvements and how could this work be altered to be used in further studies and projects.

5.1. Conclusion

This work aimed to characterize fuel cell membranes that can be used as a Nafion-alternative membranes for high temperature fuel operation. High temperature operations are highly favored due to better water management, better catalyst tolerance and better kinetics. Several membranes based on PANI, IL, and ZrP were synthesized in this work. The membranes were tested for their ability to conduct ions at high temperatures in a PEMFC. Among all, the PANI/IL/ZrP composite membrane demonstrated promising results. The conductivity of the membrane reached 0.0203 S/cm at room temperature and only dropped to 0.02 S/cm at 180 ^{o}C. Besides being a conductive membrane, the slight drop confirms the high thermal stability of the membrane.

Factorial design modelling was implemented in this work to evaluate how the conductivity response would behave as a result of changing certain factors; mainly PANI, ZrP and IL concentrations in addition to the IL type and the operating temperature. It was found that there are strong relations between these factors. Among all, the concentration of IL was found to have the highest impact on the conductivity. The IL increased the mean conductivity response up to 0.0095 S/cm; contributing to almost 50% of the response as per the results from this work. Not only these factors were found important, but also the 2-way and sometimes the 3-way interactions between these factors were found to strongly affect the mean conductivity response. For instance, the interaction between IL and ZrP concentrations was found to increase the mean conductivity up to 0.015 S/cm; contributing to approximately 12% of the response.

Furthermore, this work also touched on the fuel cell performance of the developed membranes. The composite PANI/IL/ZrP membrane was able to generate a current density up to 0.1 A/cm^2 at a potential of 0.54 V at room temperature. The current density value dropped to its half at 180 ^{o}C which was still reasonable compared to other PEMFCs and

DMFCs as shown in Figure 31. Nafion membranes for instance, shows a remarkable current density of 0.6 A/cm^2 at room temperature, however the performance drops dramatically at high temperatures [82].

The examination of the conductivity, FD and polarization curves results for the synthesized membranes, suggested that these material can be a substitute for Nafion at high temperatures. Although, at the best scenario, the conductivity was 20% of Nafion's, the synthesized membrane was thermally more stable and can withstand dehydration and water content issues. This can be confirmed by the interaction plot between temperature and IL (BD) in the 2^{nd} FD, which showed that it causes an actual increase in the mean conductivity response.

In general, the FD modelling provided more understanding of the factors included in this synthesis; how they are affecting the mean conductivity response and how the predictions fit the model an can be compared to experimental data. The theoretical cell performance predictions were also very reasonable and confirmed that the synthesized membranes have the potential to be used as a substitute for Nafion.

5.2. Future Work

In the future, this work may be used as a reference for other potential projects. This model can be altered to test several of other factors and how they may affect the cell performance or the membrane conductivity. Some of these factors may include the thickness of the membrane, the addition of other types of ILs, the backpressure of the cathode and relative humidity. Other projects may involve harvesting the fuel cell energy from the high temperature operation and utilizing it in generating steams that can turbines or be used in power industries. A water jacket can be used around the fuel cell to recover the heat.

Furthermore, one may use factorial design modelling as reference to optimize his experimental work. The factorial design can target a certain value within the given boundaries; providing the exact conditions of each factor that can be used. Once obtaining this data from the model, a verification may be done experimentally. Additionally, an

actual fuel cell need to be fabricated using the materials suggested in this work. This work provides core information that will assist in designing industrial fuel cells.

References

[1] I. Dincer, "Hydrogen and Fuel Cell Technologies for Sustainable Future," *Jordan Journal of Mechanical and Industrial Engineering*, vol. 2, no. 1, pp. 1-14, 2008.

[2] R. Raza., N. Akram, M. Javed, A. Rafique, K. Ullah, A. Ali, M. Saleem and R. Ahmed, "Fuel cell technology for sustainable development in Pakistan – An over-view," *Renewable and Sustainable Energy Reviews*, vol. 53, pp. 450-461, 2016.

[3] T. N. Atalla and L. C. Hunt, "Modelling residential electricity demand in the GCC countries," *Energy Economics*, vol. 59, pp. 149-158, 2016.

[4] S. L. Chavan and D. B. Talange, "Modeling and performance evaluation of PEM fuel cell by controlling its input parameters," *Energy*, vol. 138, pp. 437-445, 2017.

[5] J. Larminie and A. Dicks, "Fuelling Fuel Cells," in *Fuel Cell Systems Explained*, Hoboken: John Wiley & Sons, Incorporated, 2013, ch. 3, pp. 229–308.

[6] O. Z. Sharaf and M. F. Orhan, "An overview of fuel cell technology: Fundamentals and applications," *Renewable and Sustainable Energy Reviews*, vol. 32, pp. 810-853, 2014.

[7] B. Chen, Y. Cai, J. Shen, Z. Tu, and S. H. Chan, "Performance degradation of a proton exchange membrane fuel cell with dead-ended cathode and anode," *Applied Thermal Engineering*, vol. 132, pp. 80-86, 2018.

[8] L. F. Brown, "A comparative study of fuels for on-board hydrogen production for fuel-cell-powered automobiles," *International Journal of Hydrogen Energy*, vol. 26, no. 4, pp. 381-397, 2001.

[9] R. Jiang, H. R. Kunz, and J. M. Fenton, "Composite silica/Nafion® membranes prepared by tetraethylorthosilicate sol–gel reaction and solution casting for direct methanol fuel cells," *Journal of Membrane Science*, vol. 272, no. 1, pp. 116-124, 2006.

[10] T. Husaini, W. R. W. Daud, Z. Yaakob, and E. H. Majlan, "Preparation and characterization of low temperature PTFE-Nafion composite membranes for hydrogen production," *International Journal of Hydrogen Energy*, vol. 40, no. 32, pp. 10072-10080, 2015.

[11] R. E. Rosli, A.B. Sulong, W.R.W. Daud, M.A. Zulkifley, T. Husaini, M. Rosli, E.H. Majlan and M.A. Haque, "A review of high-temperature proton exchange membrane fuel cell (HT-PEMFC) system," *International Journal of Hydrogen Energy*, vol. 42, no. 14, pp. 9293-9314, 2017.

[12] J. Zhang, Z. Xie, J. Zhang, Y. Tang, C. Song, T. Navessin, Z. Shi, D. Song, H. Wang, D. Wilkinson, Z. Liu and S. Holdcroft, "High temperature PEM fuel cells," *Journal of Power Sources*, vol. 160, no. 2, pp. 872-891, 2006.

[13] J. Jagur-Grodzinski, "Polymeric materials for fuel cells: concise review of recent studies," *Polymers for Advanced Technologies*, vol. 18, no. 10, pp. 785-799, 2007.

[14] H. Pu, "Polymers for New Types of Fuel Cells," *Polymers for PEM Fuel Cells*, vol. 4, pp. 360-406, 2014.

[15] K. Dutta, S. Das, and P. P. Kundu, "Partially sulfonated polyaniline induced high ion-exchange capacity and selectivity of Nafion membrane for application in direct methanol fuel cells," *Journal of Membrane Science*, vol. 473, pp. 94-101, 2015.

[16] M. Casciola, "From layered zirconium phosphates and phosphonates to nanofillers for ionomeric membranes," *Solid State Ionics,* vol. 336, pp. 1-10, 2019.
[17] J. Maiti, N. Kakati, S. P. Woo, and Y. S. Yoon, "Nafion® based hybrid composite membrane containing GO and dihydrogen phosphate functionalized ionic liquid for high temperature polymer electrolyte membrane fuel cell," *Composites Science and Technology,* vol. 155, pp. 189-196, 2018.
[18] S. Bilal, S. Gul, R. Holze, and A.-u.-H. A. Shah, "An impressive emulsion polymerization route for the synthesis of highly soluble and conducting polyaniline salts," *Synthetic Metals,* vol. 206, pp. 131-144, 2015.
[19] Z. A. Boeva and V. G. Sergeyev, "Polyaniline: Synthesis, properties, and application," *Polymer Science Series C,* vol. 56, no. 1, pp. 144-153, 2014.
[20] M. Bláha, M. Trchová, P. Bober, Z. Morávková, Z. D. Zujovic, S. K. Filippov, J. Prokeš, J. Pilař and J. Stejskal, "Structure and properties of polyaniline interacting with H-phosphonates," *Synthetic Metals,* vol. 232, pp. 79-86, 2017.
[21] J. Huang, "Syntheses and applications of conducting polymer polyaniline nanofibers," *Pure Applied Chemistry,* vol. 78, pp. 15-27, 2006
[22] K. Lee, S. Cho, S. Heum Park, A. J. Heeger, C.-W. Lee, and S.-H. Lee, "Metallic transport in polyaniline," *Nature,* vol. 441, p. 65, 2006.
[23] N. Gospodinova, D. Ivanov, D. Anokhin, L. Mihai, L. Vidal, S. Brun, J. Romanova and A. Tadjer, "Unprecedented Route to Ordered Polyaniline: Direct Synthesis of Highly Crystalline Fibrillar Films with Strong π-π Stacking Alignment," *Macromolecular rapid communications,* vol. 30, pp. 29-33, 2009.
[24] D. Coltevieille, A. Le Méhauté, C. Challioui, P. Mirebeau, and J. N. Demay, "Industrial applications of polyaniline," *Synthetic Metals,* vol. 101, no. 1, pp. 703-704, 1999.
[25] F. D. R. Amado and S. Krishnamurthy, "Synthesis and characterisation of polyaniline (PAni) membranes for fuel cell," *Advanced Materials Letters,* vol. 7, pp. 719-722, 2016.
[26] H. Wang, J. Lin, and Z. X. Shen, "Polyaniline (PANi) based electrode materials for energy storage and conversion," *Journal of Science: Advanced Materials and Devices,* vol. 1, no. 3, pp. 225-255, 2016.
[27] G. Alberti, R. Vivani, R. K. Biswas, and S. Murcia-Mascarós, "Preparation and some properties of γ-zirconium phosphate benzenephosphonate," *Reactive Polymers,* vol. 19, pp. 1-12, 1993.
[28] H. Mohammed, A. Al-Othman, P. Nancarrow, Y. Elsayed, and M. Tawalbeh, "Enhanced proton conduction in zirconium phosphate/ionic liquids materials for high-temperature fuel cells," *International Journal of Hydrogen Energy,* vol. 26, pp. 280-286, 2019.
[29] D. Avdibegović, W. Zhang, J. Xu, M. Regadío, R. Koivula, and K. Binnemans, "Selective ion-exchange separation of scandium(III) over iron(III) by crystalline α-zirconium phosphate platelets under acidic conditions," *Separation and Purification Technology,* vol. 215, pp. 81-90, 2019.
[30] Y. Du, F. Deng, X. Jiang, H. Ji, D. Yu, W. Wang, B. Sun and M. Zhu, "Preparation and performance of lipophilic α-zirconium phosphate with high thermal stability and its application in thermal-plastic polymers," *Progress in Natural Science: Materials International,* vol. 25, pp. 503-511, 2015.

[31] Q. Li, R. He, J. O. Jensen, and N. J. Bjerrum, "Approaches and Recent Development of Polymer Electrolyte Membranes for Fuel Cells Operating above 100 °C," *Chemistry of Materials*, vol. 15, no. 26, pp. 4896-4915, 2003.

[32] G. Alberti and E. Torracca, "Crystalline insoluble salts of polybasic metals - II. Synthesis of crystalline zirconium or titanium phosphate by direct precipitation," *Journal of Inorganic and Nuclear Chemistry*, vol. 30, no. 1, pp. 317-318, 1968.

[33] H. Xiao and S. Liu, "Zirconium phosphate (ZrP)-based functional materials: Synthesis, properties and applications," *Materials & Design*, vol. 155, pp. 19-35, 2018.

[34] M. Díaz, A. Ortiz, and I. Ortiz, "Progress in the use of ionic liquids as electrolyte membranes in fuel cells," *Journal of Membrane Science*, vol. 469, pp. 379-396, 2014.

[35] A. Fernicola, B. Scrosati, and H. Ohno, "Potentialities of ionic liquids as new electrolyte media in advanced electrochemical devices," *Ionics*, vol. 12, no. 2, pp. 95-102, 2006.

[36] Q. Li, J. O. Jensen, R. F. Savinell, and N. J. Bjerrum, "High temperature proton exchange membranes based on polybenzimidazoles for fuel cells," *Progress in Polymer Science*, vol. 34, no. 5, pp. 449-477, 2009.

[37] J. S. Wainright, J. T. Wang, D. Weng, R. Savinell, and M. Litt, "Acid-Doped Polybenzimidazoles: A New Polymer Electrolyte," *Journal of The Electrochemical Society*, vol. 142, no. 7, pp. 121-123, 1995.

[38] J. T. Wang, R. F. Savinell, J. Wainright, M. Litt, and H. Yu, "A H2O2 fuel cell using acid doped polybenzimidazole as polymer electrolyte," *Electrochimica Acta*, vol. 41, no. 2, pp. 193-197, 1996.

[39] D. Aili, L. N. Cleemann, Q. Li, J. O. Jensen, E. Christensen, and N. J. Bjerrum, "Thermal curing of PBI membranes for high temperature PEM fuel cells," *Journal of Materials Chemistry*, vol. 22, no. 12, pp. 5444-5453, 2012.

[40] J. Hu, H. Zhang, Y. Zhai, G. Liu, and B. Yi, "500h Continuous aging life test on PBI/H3PO4 high-temperature PEMFC," *International Journal of Hydrogen Energy*, vol. 31, no. 13, pp. 1855-1862, 2006.

[41] X. Tian, S. Wang, J. Li, F. Liu, X. Wang, H. Chen, H. Ni and Z. Wang, "Composite membranes based on polybenzimidazole and ionic liquid functional Si–O–Si network for HT-PEMFC applications," *International Journal of Hydrogen Energy*, vol. 42, no. 34, pp. 21913-21921, 2017.

[42] X. Bao, F. Zhang, and Q. Liu, "Sulfonated poly(2,5-benzimidazole) (ABPBI)/ MMT/ ionic liquids composite membranes for high temperature PEM applications," *International Journal of Hydrogen Energy*, vol. 40, no. 46, pp. 16767-16774, 2015.

[43] P. Muthuraja, S. Prakash, V. M. Shanmugam, S. Radhakrsihnan, and P. Manisankar, "Novel perovskite structured calcium titanate-PBI composite membranes for high-temperature PEM fuel cells: Synthesis and characterizations," *International Journal of Hydrogen Energy*, vol. 43, no. 9, pp. 4763-4772, 2018.

[44] J.-D. Kim, A. Donnadio, M.-S. Jun, and M. L. Di Vona, "Crosslinked SPES-SPPSU membranes for high temperature PEMFCs," *International Journal of Hydrogen Energy*, vol. 38, no. 3, pp. 1517-1523, 2013.

[45] A. Iulianelli, I. Gatto, E. Passalacqua, F. Trotta, M. Biasizzo, and A. Basile, "Proton conducting membranes based on sulfonated PEEK-WC polymer for PEMFCs," *International Journal of Hydrogen Energy,* vol. 38, no. 36, pp. 16642-16648, 2013.
[46] M. Song, X. Lu, Z. Li, G. Liu, X. Yin, and Y. Wang, "Compatible ionic crosslinking composite membranes based on SPEEK and PBI for high temperature proton exchange membranes," *International Journal of Hydrogen Energy,* vol. 41, no. 28, pp. 12069-12081, 2016.
[47] X. Xu, R. Li, C. Tang, H. Wang, X. Zhuang, Y. Liu, W. Kang and L. Shi, "Cellulose nanofiber-embedded sulfonated poly (ether sulfone) membranes for proton exchange membrane fuel cells," *Carbohydrate Polymers,* vol. 184, pp. 299-306, 2018.
[48] C. Ni, Y. Wei, Q. Hu, X. Li, B. Liu, Q. Zhao, M. Zhang, Y. Li and W. Hu, "Nanocystalline cellulose reinforced sulfonated fluorenyl-containing polyaryletherketones for proton exchange membranes," *Solid State Ionics,* vol. 297, pp. 29-35, 2016.
[49] Z. Yang, D. H. Coutinho, R. Sulfstede, K. J. Balkus, and J. P. Ferraris, "Proton conductivity of acid-doped meta-polyaniline," *Journal of Membrane Science,* vol. 313, no. 1, pp. 86-90, 2008.
[50] C. Zhao, H. Lin, Q. Zhang, and H. Na, "Layer-by-layer self-assembly of polyaniline on sulfonated poly(arylene ether ketone) membrane with high proton conductivity and low methanol crossover," *International Journal of Hydrogen Energy,* vol. 35, no. 19, pp. 10482-10488, 2010.
[51] P. Sun, Z. Li, S. Wang, and X. Yin, "Performance enhancement of polybenzimidazole based high temperature proton exchange membranes with multifunctional crosslinker and highly sulfonated polyaniline," *Journal of Membrane Science,* vol. 549, pp. 660-669, 2018.
[52] J. Stejskal, J. Dybal, and M. Trchová, "The material combining conducting polymer and ionic liquid: Hydrogen bonding interactions between polyaniline and imidazolium salt," *Synthetic Metals,* vol. 197, pp. 168-174, 2014.
[53] R. Escudero-Cid, M. Montiel, L. Sotomayor, B. Loureiro, E. Fatás, and P. Ocón, "Evaluation of polyaniline-Nafion® composite membranes for direct methanol fuel cells durability tests," *International Journal of Hydrogen Energy,* vol. 40, no. 25, pp. 8182-8192, 2015.
[54] J. Yang, P. K. Shen, J. Varcoe, and Z. Wei, "Nafion/polyaniline composite membranes specifically designed to allow proton exchange membrane fuel cells operation at low humidity," *Journal of Power Sources,* vol. 189, no. 2, pp. 1016-1019, 2009.
[55] F. A. Zakil, S. K. Kamarudin, and S. Basri, "Modified Nafion membranes for direct alcohol fuel cells: An overview," *Renewable and Sustainable Energy Reviews,* vol. 65, pp. 841-852, 2016.
[56] M. F. A. Kamaroddin *et al.,* "Phosphoric acid doped composite proton exchange membrane for hydrogen production in medium-temperature copper chloride electrolysis," *International Journal of Hydrogen Energy,* vol. 45, no. 42, pp. 22209-22222, 2020.
[57] C. Yang, S. Srinivasan, A. S. Aricò, V. Baglio, and V. Antonucci, "Composite Nafion/Zirconium Phosphate Membranes for Direct Methanol Fuel Cell Operation

at High Temperature," *Electrochemical and Solid State Letters*, vol. 4, pp. 162-174 2001.

[58] A. Ozden, M. Ercelik, Y. Ozdemir, Y. Devrim, and C. O. Colpan, "Enhancement of direct methanol fuel cell performance through the inclusion of zirconium phosphate," *International Journal of Hydrogen Energy*, vol. 42, no. 33, pp. 21501-21517, 2017.

[59] J. Lu, F. Yan, and J. Texter, "Advanced applications of ionic liquids in polymer science," *Progress in Polymer Science*, vol. 34, no. 5, pp. 431-448, 2009.

[60] S. Rogalsky, J. Bardeau, S. Makhno, N. Babkina, O. Tarasyuk, T. Cherniavska, I. Orlovska, N. Kozyrovska and O. Brovko, "New proton conducting membrane based on bacterial cellulose/polyaniline nanocomposite film impregnated with guanidinium-based ionic liquid," *Polymer*, vol. 142, pp. 183-195, 2018.

[61] A. Al-Othman, A. Y. Tremblay, W. Pell, Y. Liu, B. A. Peppley, and M. Ternan, "The effect of glycerol on the conductivity of Nafion-free ZrP/PTFE composite membrane electrolytes for direct hydrocarbon fuel cells," *Journal of Power Sources*, vol. 199, pp. 14-21, 2012.

[62] S. Endoo, K. Pruksathorn, and P. Piumsomboon, "Identification of the key variables in membrane electrode preparation for PEM fuel cells by a factorial design," *Renewable Energy*, vol. 35, no. 4, pp. 807-813, 2010.

[63] L. Z. Garamszegi and P. de Villemereuil, "Perturbations on the uniform distribution of p-values can lead to misleading inferences from null-hypothesis testing," *Trends in Neuroscience and Education*, vol. 8-9, pp. 18-27, 2017.

[64] R. C. Dante, J. L. Escamilla, V. Madrigal, T. Theuss, Juan. Calderón, O. Solorza and R. Rivera, "Fractional factorial design of experiments for PEM fuel cell performances improvement," *International Journal of Hydrogen Energy*, vol. 28, no. 3, pp. 343-348, 2003.

[65] S.-J. Cheng, J.-M. Miao, and S.-J. Wu, "Investigating the effects of operational factors on PEMFC performance based on CFD simulations using a three-level full-factorial design," *Renewable Energy*, vol. 39, no. 1, pp. 250-260, 2012.

[66] J.-H. Kim, M. Kawai, S. Yonezawa, and M. Takashima, "Improved thermal stability of crosslinked PTFE using fluorine gas treatment," *Journal of Fluorine Chemistry*, vol. 129, no. 7, pp. 654-657, 2008.

[67] A. M. Youssef, S. Kamel, M. El-Sakhawy, and M. A. El Samahy, "Structural and electrical properties of paper–polyaniline composite," *Carbohydrate Polymers*, vol. 90, no. 2, pp. 1003-1007, 2012.

[68] S. Madani, R. Gheshlaghi, M. A. Mahdavi, M. Sobhani, and A. Elkamel, "Optimization of the performance of a double-chamber microbial fuel cell through factorial design of experiments and response surface methodology," *Fuel*, vol. 150, pp. 434-440, 2015.

[69] M. A. Nemeth, "Design and Analysis in Chemical Research," *Technometrics*, vol. 44, no. 2, pp. 190-191, 2002.

[70] W. A. Jensen, "DOE Simplified: Practical Tools for Effective Experimentation, Second Edition," *Journal of Quality Technology*, vol. 40, no. 1, pp. 124-125, 2008.

[71] D. C. Montgomery, *Design and Analysis of Experiments*, 8th Edition. Hoboken: John Wiley & Sons, Incorporated, 2012, pp. 125-130.

[72] K. A. I. L. Wijewardena Gamalath and B. M. P. Peiris, "Theoretical Approach to the Physics of Fuel Cells," *International Letters of Chemistry, Physics and Astronomy,* vol. 2, pp. 15-27, 2012.

[73] Z. Tshemese, "Progress in Green Solvents for the Stabilisation of Nanomaterials: Imidazolium Based Ionic Liquids," in *Recent Advances in Ionic liquids*, London: IntechOpen, 2018, ch. 6, pp. 480-532.

[74] K. Paduszyński and U. Domańska, "Viscosity of Ionic Liquids: An Extensive Database and a New Group Contribution Model Based on a Feed-Forward Artificial Neural Network," *Journal of Chemical Information and Modeling,* vol. 54, no. 5, pp. 1311-1324, 2014.

[75] F. Nastase, "Polyaniline," in *From Synthesis to Practical Applications*, London: IntechOpen, 2019, ch.1, pp. 18-65.

[76] J. Prokeš, M. Trchová, D. r. Hlavatá, and J. Stejskal, "Conductivity ageing in temperature-cycled polyaniline," *Polymer Degradation and Stability,* vol. 78, no. 2, pp. 393-401, 2002.

[77] F. Treish, R. Elmehdawi, A. Eldewik, and K. Kreddan, "Polyaniline α-Zirconium Phosphate Membrane," *University Bulletin,* vol. 11, pp. 1-16, 2009.

[78] H. Gharibi, M. Zhiani, A. Entezami, R. abdullah mirzaie, M. Kheirmand, and K. Kakaei, "Study of polyaniline doped with trifluoromethane sulfonic acid in gas-diffusion electrodes for proton-exchange membrane fuel cells," *Journal of Power Sources,* vol. 155, pp. 138-144, 2006.

[79] Ó. González-Espasandín, T. J. Leo, M. A. Raso, and E. Navarro, "Direct methanol fuel cell (DMFC) and H2 proton exchange membrane fuel (PEMFC/H2) cell performance under atmospheric flight conditions of Unmanned Aerial Vehicles," *Renewable Energy,* vol. 130, pp. 762-773, 2019.

[80] M. Imran, T. Li, X. wu, K. Sammed, and G. He, "Sulfonated Polybenzimidazole/amine functionalized titanium dioxide (sPBI/AFT) composite electrolyte membranes for high temperature proton exchange membrane fuel cells usage," *Chinese Journal of Chemical Engineering,* vol. 28, no. 9, pp. 2425-2437, 2020.

[81] L.-C. Chen, T. Yu, H.-L. Lin, and S.-H. Yeh, "Nafion/PTFE and zirconium phosphate modified Nafion/PTFE composite membranes for direct methanol fuel cells," *Journal of Membrane Science,* vol. 307, pp. 10-20, 2008.

[82] M. Casciola, G. Alberti, M. Sganappa, and R. Narducci, "On the decay of Nafion proton conductivity at high temperature and relative humidity," *Journal of Power Sources,* vol. 162, no. 1, pp. 141-145, 2006.

[83] Suryani, Y.-N. Chang, J.-Y. Lai, and Y.-L. Liu, "Polybenzimidazole (PBI)-functionalized silica nanoparticles modified PBI nanocomposite membranes for proton exchange membranes fuel cells," *Journal of Membrane Science,* vol. 403-404, pp. 1-7, 2012.

[84] S. M. J. Zaidi, "Preparation and characterization of composite membranes using blends of SPEEK/PBI with boron phosphate," *Electrochimica Acta,* vol. 50, no. 24, pp. 4771-4777, 2005.

Appendix A

Since each experiment was repeated three times, instead of having 2n number of experiments, 3×2^n experiments were obtained for each factorial design model. The experiments were ran randomly and the response was observed and recorded accordingly. Table A.1 and Table A.2 present the full data for both factorial design models conducted on this work.

Table A. 1: Full factorial design data for the 1st model.

Std. order	Run order	PANI (wt%) (A)	IL type (E)	Conductivity (S/cm)
1	8	0.61	Diethylmethylammonium Methanesulfonate	0.0033
2	5	1.22	Diethylmethylammonium Methanesulfonate	0.0028
3	3	0.61	1-Hexyl-3-Methylimidazolium Tricyanomethanide	0.009
4	9	1.22	1-Hexyl-3-Methylimidazolium Tricyanomethanide	0.0085
5	7	0.61	Diethylmethylammonium Methanesulfonate	0.004
6	6	1.22	Diethylmethylammonium Methanesulfonate	0.0034
7	11	0.61	1-Hexyl-3-Methylimidazolium Tricyanomethanide	0.0088
8	1	1.22	1-Hexyl-3-Methylimidazolium Tricyanomethanide	0.0092
9	2	0.61	Diethylmethylammonium Methanesulfonate	0.0034
10	10	1.22	Diethylmethylammonium Methanesulfonate	0.0022
11	12	0.61	1-Hexyl-3-Methylimidazolium Tricyanomethanide	0.0097
12	4	1.22	1-Hexyl-3-Methylimidazolium Tricyanomethanide	0.0079

Table A. 2: Full factorial design data for the 2nd model.

Std. order	Run order	PANI (wt%) (A)	IL (wt%) (B)	ZrP (wt%) (C)	Temperature (ºC) (D)	Conductivity (S/cm)
1	44	0.61	0	0	25	0.0009
2	42	1.22	0	0	25	0.0008
3	8	0.61	2.5	0	25	0.0088
4	36	1.22	2.5	0	25	0.0085
5	39	0.61	0	0.61	25	0.0008
6	16	1.22	0	0.61	25	0.00051
7	25	0.61	2.5	0.61	25	0.02
8	30	1.22	2.5	0.61	25	0.01
9	1	0.61	0	0	180	0.00018
10	45	1.22	0	0	180	0.000152
11	28	0.61	2.5	0	180	0.0019257
12	21	1.22	2.5	0	180	0.00179
13	24	0.61	0	0.61	180	0.000159
14	35	1.22	0	0.61	180	0.0001077
15	46	0.61	2.5	0.61	180	0.021
16	29	1.22	2.5	0.61	180	0.00837
17	43	0.61	0	0	25	0.00096
18	31	1.22	0	0	25	0.00084
19	5	0.61	2.5	0	25	0.009
20	11	1.22	2.5	0	25	0.0092
21	2	0.61	0	0.61	25	0.00075
22	4	1.22	0	0.61	25	0.00053
23	19	0.61	2.5	0.61	25	0.019
24	9	1.22	2.5	0.61	25	0.01
25	40	0.61	0	0	180	0.000171
26	22	1.22	0	0	180	0.000168
27	33	0.61	2.5	0	180	0.0017423
28	13	1.22	2.5	0	180	0.001706
29	47	0.61	0	0.61	180	0.000144
30	34	1.22	0	0.61	180	0.00011908
31	48	0.61	2.5	0.61	180	0.019
32	38	1.22	2.5	0.61	180	0.00795
33	20	0.61	0	0	25	0.00084
34	23	1.22	0	0	25	0.00076
35	41	0.61	2.5	0	25	0.0097
36	15	1.22	2.5	0	25	0.0079
37	12	0.61	0	0.61	25	0.00072
38	7	1.22	0	0.61	25	0.00051

39	18	0.61	2.5	0.61	25	0.022
40	14	1.22	2.5	0.61	25	0.0071
41	17	0.61	0	0	180	0.00019
42	10	1.22	0	0	180	0.00016
43	26	0.61	2.5	0	180	0.001834
44	32	1.22	2.5	0	180	0.0016207
45	3	0.61	0	0.61	180	0.0001514
46	27	1.22	0	0.61	180	0.0001134
47	6	0.61	2.5	0.61	180	0.02
48	37	1.22	2.5	0.61	180	0.00879

Appendix B

According to Nastase, the conductivity of pure PANI at high temperatures would be roughly 5 times lower than its value at room temperature. Therefore, considering that this assumption applies at 180 oC, the conductivity of 0.61 wt% PANI and 1.22 wt% PANI would be calculated using Equation A.1 and Equation A.2 respectively:

$$0.61\ wt\%\ PANI\ _{180} = \frac{0.61\ wt\%\ PANI\ _{25}}{5} \tag{A.1}$$

$$0.61\ wt\%\ PANI\ _{180} = \frac{0.0009}{5} = 0.000184\ S/cm$$

$$1.22\ wt\%\ PANI\ _{180} = \frac{1.22\ wt\%\ PANI\ _{25}}{5} \tag{A.2}$$

$$1.22\ wt\%\ PANI\ _{180} = \frac{0.0008}{5} = 0.00016\ S/cm$$

For the PANI/IL membranes, as assumed earlier, one must account for the change due to the IL effect. The change effect due to addition of IL (ΔE_{IL}) in 0.61 wt% PANI and 1.22 wt% PANI can be calculated as:

$$\Delta E_{IL,0.61\%PANI} = \frac{(0.61{:}2.5\ \text{wt\%})\ \frac{PANI}{IL}_{25}}{0.61\ wt\%\ PANI\ _{25}} \tag{A.3}$$

$$\Delta E_{IL,0.61\%PANI} = \frac{0.00917}{0.0009} = \ 10.19$$

$$\Delta E_{IL,1.22\%\ PANI} = \frac{(1.22{:}2.5\ \text{wt\%})\ PANI/IL\ _{25}}{1.22\ wt\%\ PANI\ _{25}} \tag{A.4}$$

$$\Delta E_{IL,1.22\%\ PANI} == \frac{0.00853}{0.0008} = \ 10.63$$

Therefore, the PANI/IL membranes' conductivity at 180 ºC can now be calculated as:

$$(0.61:2.5\ \text{wt\%})PANI/IL_{180} = 0.61\ wt\%\ PANI_{\ 180} \times \Delta E_{IL,0.61\%\ PANI} = 0.000184 \times 10.19 = 0.00183\ S/cm$$

$$(1.22:2.5\ \text{wt\%})PANI/IL_{180} = 1.22\ wt\%\ PANI_{\ 180} \times \Delta E_{IL,1.22\%\ PANI} = 0.00016 \times 10.63 = 0.00171\ S/cm$$

Similar to the PANI/IL membranes, PANI/ZrP membranes must also consider the change due to the ZrP effect. The change effect due to the addition of ZrP (ΔE_{ZrP}) in 0.61 and 1.22 wt% PANI can be calculated as:

$$\Delta E_{ZrP\ 0.61\%\ PANI} = \frac{(061{:}0.61\ wt\%)\ PANI/ZrP_{25}}{0.61\ wt\%\ PANI_{\ 25}} \quad \text{(A.5)}$$

$$\Delta E_{ZrP\ 0.61\%\ PANI} == \frac{0.00076}{0.0009} = 0.84$$

$$\Delta E_{ZrP\ 1.22\%\ PANI} = \frac{(1.22{:}0.61\ wt\%)\ PANI/ZrP_{25}}{1.22\ wt\%\ PANI_{\ 25}} \quad \text{(A.6)}$$

$$\Delta E_{ZrP\ 1.22\%\ PANI} = \frac{0.00057}{0.0008} = 0.63$$

Hence, the PANI/ZrP membranes at 180 ºC can now be calculated as:

$$(0.61:0.61\ \text{wt\%})PANI/ZrP_{180} = 0.61\ wt\%\ PANI_{\ 180} \times \Delta E_{ZrP\ 0.61\%\ PANI} = 0.000184 \times 0.84 = 0.0015\ S/cm$$

$$(1.22:2.5\%\ \text{wt})PANI/ZrP_{180} = 1.22\ wt\%\ PANI_{\ 180} \times \Delta E_{ZrP\ 1.22\%\ PANI} = 0.00016 \times 0.63 = 0.0011\ S/cm$$

Finally, for the 1.22 wt% PANI/ZrP/IL composite membrane, the membrane conductivity was predicted after measuring the 0.61 wt% PANI/ZrP/IL using the high temperature test. Keeping in mind that for the later conductivity was found to be 0.020 S/cm, and considering that the effect of of the addition of both IL and ZrP ($E_{ZrP,IL,PANI}$)

would be the same at high and low temperatures, the change in conductivity may be assumed similar to the change at low temperature. In other words:

$$E_{ZrP,IL,PANI} = \frac{(1.22{:}061{:}2.5\%)PANI/ZrP/IL_{25}}{(0.61{:}061{:}2.5\%)PANI/ZrP/IL_{25}} \quad \text{(A.7)}$$

$$E_{ZrP,IL,PANI} = \frac{0.0085}{0.0203} = 0.42$$

Therefore the conductivity of the 1.22% PANI/ZrP/IL membrane at 180 ^{o}C was predicted to be:

$$(1.22{:}061{:}2.5\%)\ PANI/ZrP/IL_{180}$$
$$= (0.61{:}061{:}2.5\%)PANI/ZrP/IL_{180} \times E_{ZrP,IL,PANI} = 0.02 \times 0.42$$
$$= 0.0084\ S/cm$$

The electric conductivity (σ_e) of PANI/ZrP/IL at room and high temperatures can be predicted using similar approach. The change due to the addition of ZrP and IL in pure PANI ($E_{ZrP,IL,pure\ PANI}$) can be given by Equation A.8 below:

$$E_{ZrP,IL,pure\ PANI} = \frac{(0.61{:}061{:}2.5\%)PANI/ZrP/IL_{25}}{0.61\ wt\%\ PANI_{25}} \quad \text{(A.8)}$$

$$E_{ZrP,IL,pure\ PANI} = \frac{0.0203}{0.0009} = 22.2$$

Therefore, the electric conductivity at room temperature can be calculated as:

$$\sigma_{e,PANI,ZrP,IL,25} = \sigma_{e,PANI,25} \times E_{ZrP,IL,pure\ PANI} = 3.5 \times 22.2 = 77.7\ S/cm$$

Now, using the similarity equation (Equation A.7), the value of the electric conductivity can be given by:

$$\sigma_{e,PANI,ZrP,IL,180} = \sigma_{e,PANI,ZrP,IL,25} \times E_{ZrP,IL,PANI} = 77.7 \times 0.42 = 32.63$$

Thickness and resistance data for the synthesized membranes can be found in Table A.3 below. These data are crucial for Equation 9 and Equation 12.

Table A. 3: Resistance and Thickness data for the synthesized membranes.

Membrane type	**Temperature**	**Average Resistance**	**Average Thickness**
0.61 wt% PANI	25	54.10	0.30
1.22 wt% PANI	25	60.90	0.31
0.61 wt% PANI/HMT IL	25	5.84	0.34
1.22 wt% PANI/HMT IL	25	7.40	0.40
0.61 wt% PANI/DEMM IL	25	17.16	0.39
1.22 wt% PANI/DEMM IL	25	23.58	0.42
0.61 wt% PANI/ZrP	25	123.40	0.60
1.22 wt% PANI/ZrP	25	182.00	0.66
0.61 wt% PANI/ZrP/HMT IL	25	4.40	0.60
1.22 wt% PANI/ZrP/HMT IL	25	11.83	0.64
0.61 wt% PANI/ZrP/HMT IL	180	4.9	0.62

Vita

Ahmed Eisa was born in 1994, in Dubai, United Arab Emirates (UAE). He graduated from Al Wuhaida high school with a 99% grade average. Following his high school graduation, he joined the BSc. program in chemical engineering at the American University of Sharjah where he managed to receive his diploma by 2016.

Mr. Eisa wanted to further develop his academic knowledge and his research skills; hence he joined the MSc. program in chemical engineering at the same university by 2017, where he received a graduate teaching assistantship merit. Following his admission, Ahmed succeeded to publish two Scopus indexed journal papers.

In 2018, Ahmed managed to publish his first research; when he co-authored a research work on seawater desalination titled “Novel multi-stage flash (MSF) desalination plant driven by parabolic trough collectors and a solar pond: A simulation study in UAE”. The work was published in the Desalination journal.

In 2019, Mr. Eisa was appointed as a field consultant and a quality control inspector for Al Hamar Gulf Establishment; the developing agent for Subway in the UAE and Bahrain. He first joined the company as an intern; however, following his performance and skills, he managed to secure a full time position.

By 2020, Ahmed managed to publish his second research work; this time as a first author for a research work in membrane technology titled “Novel High Temperature Membranes Based on Polyaniline /Ionic Liquids for PEM Fuel Cells Applications”. The publication was actually based on this thesis. He also presented some of his research work in multiple conferences throughout his study period at the American University of Sharjah.